2006

Traveling Waves in a Suspension Bridge System

Robert A. Ain
University of Nevada, Las Vegas

TRAVELING WAVES IN A SUSPENSION BRIDGE SYSTEM

by

Robert A. Ain, Jr.

Bachelor of Science
United States Air Force Academy
1974

A thesis submitted in partial fulfillment
of the requirements for the

Master of Science Degree in Mathematical Sciences
Department of Mathematical Sciences
College of Sciences

Graduate College
University of Nevada, Las Vegas
May 2006

UNLV
UNIVERSITY OF NEVADA LAS VEGAS

Thesis Approval
The Graduate College
University of Nevada, Las Vegas

April 7, 2006

The Thesis prepared by

Robert A. Ain, Jr.

Entitled

"Traveling Waves in a Suspension Bridge System"

is approved in partial fulfillment of the requirements for the degree of

Master of Science in Mathematical Sciences

Examination Committee Chair

Dean of the Graduate College

Examination Committee Member

Examination Committee Member

Graduate College Faculty Representative

1017-53

ABSTRACT

Traveling Waves in a Suspension Bridge System

by

Robert A. Ain, Jr.

Dr. Zhonghai Ding, Examination Committee Chair
Associate Professor of Mathematics
University of Nevada, Las Vegas

In this thesis, we study the traveling waves in a Lazer-McKenna suspension bridge system which is governed by two coupled nonlinear beam and wave equations. The Lazer-McKenna suspension bridge system describes the vertical deflections in the roadbed and supporting cable of a suspension bridge. Based on some basic analysis on the system, we are able to compute traveling waves numerically by using MAPLE. Multiple large-amplitude traveling waves are obtained. The graphs of various traveling waves are displayed and discussed.

TABLE OF CONTENTS

LIST OF FIGURES

ACKNOWLEDGEMENTS

The opportunity to study mathematics at this stage of my life is certainly a blessing. The number of people that deserve my thanks in this endeavor are too many to list here, but I will go out on a limb and acknowledge some who have been particularly significant.

The first thanks go to my advisor and thesis committee chair, Dr. Zhonghai Ding. In the classroom, in his office, even during dark times when I was not sure I could make it, he always encouraged me and had faith that I could. It is without exaggeration that I say I couldn't have done this without his help.

Next, I would be remiss if I overlooked the other members of the thesis committee, Dr. Yitun Chen, Dr. David Costa, and Dr. George Miel. No matter how hard I worked to make this thesis perfectly clear, it is still a daunting task to review and evaluate this much work. Thank you.

My professors at UNLV have all given me encouragement in addition to the considerable mathematical knowledge they were able to pass on to me. In addition, members of the faculty that weren't even my teachers extended themselves and helped me in this regard. Thank you one and all.

Scholarship is seldom a solitary task. I have lost count of the number of times one of my fellow graduate students helped me figure out something I needed to know. I certainly appreciate your help, and cherish your friendship.

Finally, my wife, Debbie, and my family have been more than supportive, and have given me perspective about my entire life, including my pursuits as a student. You are the best, and I cherish you!

CHAPTER 1

INTRODUCTION

Bridges are one of the most important artifacts of civilization. From the first time one of our distant ancestors decided to walk across a creek on a fallen log instead of wading and getting wet, bridges have been an important part of human existence. As man developed technology, the materials and methods of bridge construction improved.

Reasonably substantial suspension bridges have been documented as far back as about 206 B.C. in China, but western engineers really started using these designs in the eighteenth and nineteenth centuries. When steel became a preferred material, suspension bridges became the preferred design when spanning relatively long distances. However, the advantages of the suspension bridges were sometimes (maybe often) overtaken by idiosyncrasies characteristic to the design. Many had disconcerting dynamic behavior, and more than a few failed when that behavior became excessive [19]. It has been known that repeated large amplitude oscillations can cause mechanical fatigues in suspension bridges. The study of these destructive oscillations is therefore fundamental in preventing the possible failures of suspension bridges. This thesis studies the traveling waves in suspension bridges.

Figure 1.1. Tacoma Narrow Bridge before collapse. (WSDOT photo).

The classic event regarding the destructive large amplitude oscillations in suspension bridges was the collapse of the Tacoma Narrows suspension bridge (Figure 1.1) in November 1940. This particular bridge was the epitome of lightweight design, and its inherent flexibility was part of its downfall. While there were other suspension bridge failures before this one, it is fair to say that this event opened the inquiry into the mathematical modeling and analysis of suspension bridge systems. The behaviors of the Tacoma Narrows suspension bridge were pretty well documented, and a well-qualified panel of engineers and scientists looked into the failure of the bridge for the government in the early 1940s [3]. An initial analysis, attributed to von Karman and others [3], suggested that the dynamics of the bridge (Figure 1.2) were attributable to resonance. This explanation is not too difficult to understand, and it seemed to be a satisfactory explanation at the time. However, there are some problems with this explanation [21]. Resonance is a precise phenomenon; the conditions in the middle of a big windstorm are anything but precise. Further, the documented behavior of the

bridge indicated something else was happening. Sometimes, the Tacoma Narrows suspension bridge was calm in high winds; sometimes it was dynamic in very light winds. This discourages the idea that resonance could be the culprit. In the end, the report concludes that resonance was improbable as the cause for the failure of Tacoma Narrows suspension bridge [3].

Figure 1.2. Tacoma Narrow Bridge very shortly before collapse, November 7, 1940. Note the combination of vertical and torsional deflection that eventually caused the structure to fail. (photo:www.ketchum.org)

The initial models for suspension bridges were linear, but it turns out that they are inadequate to describe the complicated dynamics of bridge systems. Such bridge systems are fundamentally nonlinear [21], based on the fact that the forces applied to the roadbed as it flexes up are different than the forces applied when it flexes down. This can be traced back to a principle from early in my engineering education: "You can't push on a rope." The vertical stays that support the roadbed tend to restore the bed to position in tension, but do nothing in compression.

It seems that the early work on mathematical modeling and analysis was done by Bleich, McCollough, Rosecrans, and Vincent [5](1950). Their work was followed later by other researchers [1] [24-28]. Lazer and McKenna discussed and summarized the development of mathematical models for this problem in a celebrated paper [21](1990). Based on their analysis in their paper, they proposed some new nonlinear models to describe suspension bridge systems. In the first model proposed by Lazer and McKenna [21], the road is modeled by a nonlinear beam equation

$$(1.1)\quad \begin{cases} u_{tt} + EIu_{xxxx} + \delta u_t + ku^+ = W(x) + \varepsilon f(x,t) \\ u(0,t) = u(L,t) = u_{xx}(0,t) = u_{xx}(L,t) = 0 \end{cases}$$

where $u(x,t)$ is the vertical displacement of the roadbed; EI is the roadbed flexural rigidity; δ is a small viscous damping constant; k is the Hooke's constant for the stays supporting the roadbed; $W(x)$ is the weight per unit length of the roadbed; and $\varepsilon f(x,t)$ is the forcing term. The roadbed length is L, with both ends being simply supported. The one-dimensional Lazer-McKenna suspension bridge equation describes movement of the roadbed based on nonlinear support from a cable that is assumed fixed.

Large amplitude periodic solutions were found by Lazer and McKenna [21](1987). Since the pioneering work by Lazer and McKenna, quite a few papers have been published on the study of the one-dimensional Lazer-McKenna suspension bridge equation. Glover, Lazer, and McKenna showed existence and stability of large amplitude nonlinear oscillations [14](1989). Choi, Jung and McKenna approached the problem by using a variational reduction

method [7](1993). Humphreys computed numerical solutions of (1.1) by a numerical mountain pass algorithm [16](1997). Humphreys and McKenna proved the existence of multiple periodic solutions [17](1999).

The second Lazer-McKenna model is somewhat more complex. It considers motion in the supporting cable, as well as the roadbed. Clearly, this is a more accurate description of the actual motion of a suspension bridge. The second model is governed by the coupled beam and wave equations

$$(1.2)\quad \begin{cases} m_c u_{tt} - Q u_{xx} + \delta_1 u_t - k(w-u)^+ = \varepsilon f_1(x,t) \\ m_b w_{tt} + EI w_{xxxx} + \delta_2 w_t + k(w-u)^+ = W_1 \\ w(0) = w(L,t) = w_{xx}(0) = w_{xx}(L,t) = u(0) = u(L,t) = 0 \end{cases}$$

with m_c and m_b denote the mass densities of the supporting cable and roadbed; u and w denote the vertical displacements of the cable and roadbed; and δ_1 and δ_2 are the damping coefficients for the cable and roadbed; Q represents the coefficient of cable tensile strength; EI is the roadbed flexural rigidity; k is the Hooke's constant for the stays supporting the roadbed; $(w-u)^+$ is $\max\{(w-u),0\}$; W_1 is the incremental weight of the roadbed, which is assumed to be constant. The literature on this model is quite limited. Ahmed and Harbi [2](1998) studied the asymptotic stability of (1.2), Drabek and Leinfelder [13](1999) and Berkovits, Drabek, Leinfelder, Mustonen, and Tajcova [4](2000) studied the existence and uniqueness of the solution of (1.2) when ε is small. In a series of papers by Ding [8](2000), [9,10,11](2002), the existence of multiple periodic oscillations when $\delta_1 = \delta_2 = 0$ was studied by some nonlinear functional analysis methods.

Traveling waves in suspension bridges were observed and reported in some detail by R.G. Cone [23](1938) after observing the Golden Gate Bridge during a severe windstorm. As it turns out, both of the Lazer-McKenna models admit traveling wave solutions. McKenna and Walter [23](1990) found traveling waves numerically in the single Lazer-McKenna suspension bridge model (1.1). Chen and McKenna [6](1997) further studied the same problem and proved the existence of at least one traveling wave by a variational method. Ding [12](2003) showed that the Lazer-McKenna model (1.2) admits at least one nontrivial traveling wave by a similar approach. More recently, Horak and McKenna [15](2003) studied traveling waves in a thin plate.

The objective of this thesis is to compute numerically the traveling waves of the Lazer-McKenna suspension bridge system (1.2). Our approach to the problem is similar to the method used by McKenna and Walter [23] on the single Lazer-McKenna suspension bridge equation (1.1). We pursue analytic solutions as far as we can, then use MAPLE to compute numerical solutions.

The organization of this thesis is as follows. In Chapter 2, we set up the problem. Chapter 3 will discuss the analytic portion of the solutions. Chapter 4 will encompass the numerical work, and Chapter 5 will include the summary and recommendations for future work.

CHAPTER 2

PROBLEM DESCRIPTION

In this chapter, we will start with the Lazer-McKenna suspension bridge system, and formulate the problem.

From [21] by Lazer and McKenna, we consider:

$$(2.1)\quad \begin{cases} m_c u_{tt} - Q u_{xx} - k(w-u)^+ = m_c g & x \in \square,\ t \in \square \\ m_b u_{tt} + EI w_{xxxx} + k(w-u)^+ = m_b g & x \in \square,\ t \in \square \end{cases}$$

with m_c and m_b the masses, u and w the position functions for the cable and roadbed, respectively; Q represents the coefficient of cable tensile strength; EI is the roadbed flexural rigidity; k is the Hooke's constant for the stays supporting the roadbed; $(w-u)^+$ is $\max\{w-u, 0\}$; g is the gravity constant. From what we know about suspension bridges, it is natural to assume $m_b > m_c > 0$. To study traveling waves, assume

$$(2.2)\quad \begin{cases} u(x,t) = u_e(x) + y(x-ct) \\ w(x,t) = w_e(x) + z(x-ct) \end{cases}$$

where c is the wave speed, and $u_e(x)$ and $w_e(x)$ are the steady-state solutions of (2.1) above, i.e.,

$$(2.3)\quad \begin{cases} -Q u_{xx} - k(w-u)^+ = m_c g \\ EI w_{xxxx} + k(w-u)^+ = m_b g \end{cases}.$$

A direct calculation yields

$$(2.4)\quad \begin{cases} u_e(x) = \dfrac{-(m_c + m_b)g}{2Q}x^2 \\ w_e(x) = \dfrac{-(m_c + m_b)g}{2Q}x^2 + \dfrac{m_b g}{k} \end{cases}$$

To make our analysis easier, let $s = (x - ct)$. Thus, $y(s)$ and $z(s)$ satisfy

$$(2.5)\quad \begin{cases} (c^2 m_c - Q)y'' - k(z - y + \dfrac{m_b g}{k})^+ + \dfrac{m_b g}{k} = 0 \\ c^2 m_b z'' + EIz^{(4)} + k(z - y + \dfrac{m_b g}{k})^+ - \dfrac{m_b g}{k} = 0 \end{cases}.$$

Substitute $y = \dfrac{\tilde{y}}{k}$ and $z = \dfrac{\tilde{z}}{k}$ into (2.5) to get

$$(2.6)\quad \begin{cases} \dfrac{(c^2 m_c - Q)}{k}\tilde{y}'' - (\tilde{z} - \tilde{y} + m_b g)^+ + m_b g = 0 \\ \dfrac{c^2 m_b}{k}\tilde{z}'' + \dfrac{EI}{k}\tilde{z}^{(4)} + (\tilde{z} - \tilde{y} + m_b g)^+ - m_b g = 0 \end{cases}.$$

By substituting $\tilde{y} = m_b g\hat{y}$ and $\tilde{z} = m_b g\hat{z}$ into (2.6), we have

$$(2.7)\quad \begin{cases} \dfrac{(c^2 m_c - Q)}{k}\hat{y}'' - (\hat{z} - \hat{y} + 1)^+ + 1 = 0 \\ \dfrac{c^2 m_b}{k}\hat{z}'' + \dfrac{EI}{k}\hat{z}^{(4)} + (\hat{z} - \hat{y} + 1)^+ - 1 = 0 \end{cases}.$$

By adding the two equations in (2.7), we obtain

$$(2.8)\qquad m_b c^2 \hat{z}'' + EI\hat{z}^{(4)} + (m_c c^2 - Q)\hat{y}'' = 0.$$

Before a further discussion of solutions to (2.8), we need to specify the solutions spaces of $\hat{y}$ and $\hat{z}$. We look for solutions for $(\hat{y}, \hat{z}) \in H^2(\square) \times H^4(\square)$ where $H^2(\square)$ and $H^4(\square)$ are the Sobolev function spaces given by

$$H^2(\square) = \left\{ f \in L^2(\square) \mid f', f'' \in L^2(\square) \right\}$$
$$H^4(\square) = \left\{ f \in L^2(\square) \mid f', f'', f''', f^{(4)} \in L^2(\square) \right\}.$$

Note that $H^2(\square) \subset C(\square)$ and $H^4(\square) \subset C(\square)$. This is consistent with the fact that the boundary conditions require the functions $\hat{y}$ and $\hat{z}$, as well as their first two or four derivatives (respectively) be zero at $\pm\infty$. We also expect the functions to be continuous. By integrating (2.8), we have

$$\int_{-\infty}^{\xi} \hat{y}'' d\omega = \frac{1}{(Q - m_c c^2)} \int_{-\infty}^{\xi} \left(m_b c^2 \hat{z}'' + EI\hat{z}^{(4)} \right) d\omega$$

$$\hat{y}'(\xi) - \hat{y}'(-\infty) = \frac{1}{(Q - m_c c^2)} [m_b c^2 \hat{z}'(\xi) + EI\hat{z}'''(\xi) - m_b c^2 \hat{z}'(-\infty) - EI\hat{z}'''(-\infty)].$$

$$\hat{y}'(\xi) = \frac{1}{(Q - m_c c^2)} [m_b c^2 \hat{z}'(\xi) + EI\hat{z}'''(\xi)]$$

We repeat the process to get

$$\int_{-\infty}^{s} \hat{y}'(\xi) d\xi = \frac{1}{(Q - m_c c^2)} \int_{-\infty}^{s} [m_b c^2 \hat{z}'(\xi) + EI\hat{z}'''(\xi)] d\xi$$

$$\hat{y}(s) - \hat{y}(-\infty) = \frac{1}{(Q - m_c c^2)} [m_b c^2 \hat{z}(s) + EI\hat{z}''(s) - m_b c^2 \hat{z}(-\infty) - EI\hat{z}''(-\infty)],$$

$$(2.9)\quad \hat{y}(s) = \frac{-m_b c^2 \hat{z}(s) - EI\hat{z}''(s)}{(m_c c^2 - Q)}$$

which is well defined for $m_c c^2 - Q \neq 0$. From now on, we assume

$$(2.10)\quad 0 < c^2 < \frac{Q}{m_b + m_c}.$$

Furthermore, we assume

$$(2.11)\quad \begin{cases} \dfrac{m_b}{m_c} < \dfrac{\sqrt{kEI}}{Q - \sqrt{kEI}} & \text{if } \ 0 < k < \dfrac{Q^2}{EI} \\ \text{No condition for} & k \geq \dfrac{Q^2}{EI} \end{cases}$$

Under (2.10) and (2.11), it is proved in [12] that system (2.1) admits at least one traveling wave solution.

By substituting (2.9) into the second equation of (2.7), we obtain

$$(2.12) \quad \frac{m_b}{k} c^2 \hat{z}'' + \frac{EI}{k} \hat{z}^{(4)} + \left(\hat{z} + \frac{m_b c^2 \hat{z}(s) + EI\hat{z}''(s)}{(m_c c^2 - Q)} + 1 \right)^+ - 1 = 0 \ .$$

The above derivation indicates equations (2.9) and (2.12) are equivalent to the system (2.7). Therefore, we can find traveling waves in (2.1) by solving (2.12).

CHAPTER 3

PROBLEM ANALYSIS

Having stated the problem in a manageable way, we are now in a position to proceed with some analysis of (2.12). Our goal is to put together groups of mathematical relationships that will lead to solution by numerical computation. Along the way, we will have to consider different cases determined by different parts of the domain that have different characteristics, and also cases for different possible outcomes within a part of the domain.

We first establish two cases,

Case 1: $\dfrac{[(m_b + m_c)c^2 - Q]\hat{z} + EI\hat{z}''}{(m_c c^2 - Q)} > -1,$

where equation (2.12) becomes

$$(3.1) \quad \frac{m_b}{k} c^2 \hat{z}'' + \frac{EI}{k} \hat{z}^{(4)} + \frac{[(m_b + m_c)c^2 - Q]\hat{z} + EI\hat{z}''}{(m_c c^2 - Q)} = 0 \quad .$$

Case 2: $\dfrac{[(m_b + m_c)c^2 - Q]\hat{z} + EI\hat{z}''}{(m_c c^2 - Q)} \leq -1,$

where equation (2.12) becomes

$$(3.2) \quad \frac{m_b}{k} c^2 \hat{z}'' + \frac{EI}{k} \hat{z}^{(4)} - 1 = 0 \, .$$

3.1 Initial Analysis for Case 1.

By (3.1) we have

$$(3.3)\quad (m_c c^2 - Q)\frac{EI}{k}\hat{z}^{(4)} + ((m_c c^2 - Q)\frac{m_b}{k}c^2 + EI)\hat{z}'' + [(m_b + m_c)c^2 - Q]\hat{z} = 0 .$$

The corresponding characteristic equation is

$$(3.4)\quad (Q - m_c c^2)EI\lambda^4 + \left((Q - m_c c^2)m_b c^2 - kEI\right)\lambda^2 + k\left(Q - (m_b + m_c)c^2\right) = 0 .$$

Since (3.4) is quadratic in λ^2, apply the quadratic formula to get

$$(3.5)\quad \lambda^2 = \frac{\left(kEI - (Q - m_c c^2)m_b c^2\right) \pm \sqrt{\left((Q - m_c c^2)m_b c^2 - kEI\right)^2 - 4(Q - m_c c^2)kEI\left(Q - (m_c + m_b)c^2\right)}}{2(Q - m_c c^2)EI} .$$

To discuss the roots of λ, we let

$$(3.6)\quad \mathrm{F}_1(c^2) = kEI - (Q - m_c c^2)m_b c^2 = m_b m_c c^4 - Q m_b c^2 + kEI$$

$$(3.7)\quad \mathrm{F}_2(c^2) = \left((Q - m_c c^2)m_b c^2 - kEI\right)^2 - 4(Q - m_c c^2)kEI\left(Q - (m_c + m_b)c^2\right)$$

3.2 Analysis of $\mathrm{F}_1(c^2)$.

We need to know the sign of $\mathrm{F}_1(c^2)$ at different parts of the domain. Consider first $\mathrm{F}_1(0) = kEI$, which is positive. To consider the largest value of c^2 in the domain, recall (2.10), which gives

$$(3.8)\quad \mathrm{F}_1\left(\frac{Q}{m_b + m_c}\right) = kEI - \frac{Q^2 {m_b}^2}{\left(m_b + m_c\right)^2} .$$

Under the assumption (2.11), $F_1(\frac{Q}{m_b+m_c}) > 0$. The graph of $F_1(c^2)$ is a parabola in c^2 that opens upward and has the axis of symmetry at $c^2 = \frac{Q}{2m_c}$. Observe that $0 < c^2 < \frac{Q}{m_b+m_c} < \frac{Q}{2m_c}$, since $m_c < m_b$. Thus, $F_1(c^2) > 0$ on $\left(0, \frac{Q}{m_b+m_c}\right)$.

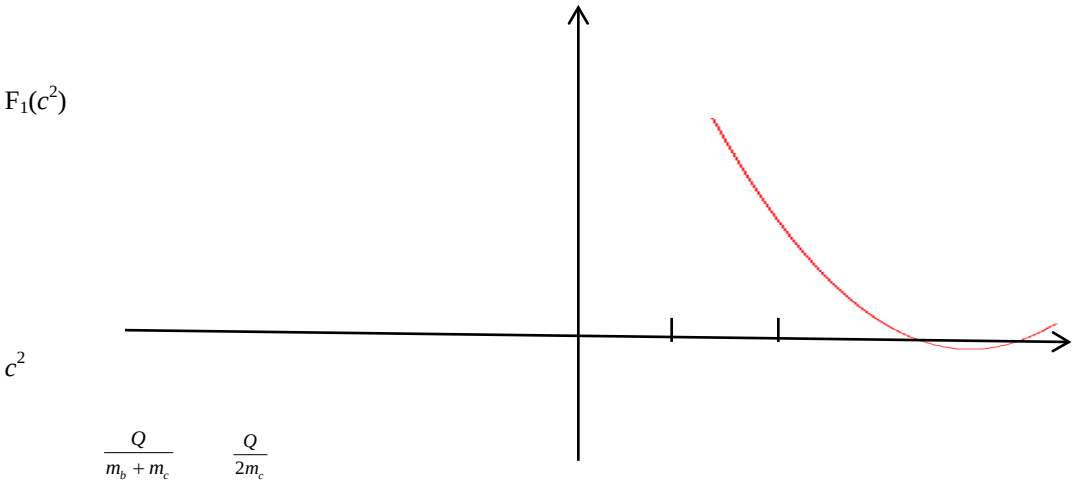

Figure 3.1. Graph of characteristics for $F_1(c^2)$.

3.3 Analysis of $F_2(c^2)$.

Now consider $F_2(c^2)$ on $\left(0, \frac{Q}{m_b+m_c}\right)$. Note that

$$\mathrm{F}_2(0) = \left(kEI\right)^2\left(1-\frac{4Q^2}{kEI}\right).$$

Thus, $\mathrm{F}_2(0) > 0$ for $k > \frac{4Q^2}{EI}$, and $\mathrm{F}_2(0) < 0$ for $k < \frac{4Q^2}{EI}$. Simplification of $\mathrm{F}_2(\frac{Q}{m_b + m_c})$ yields

$$\mathrm{F}_2(\frac{Q}{m_b + m_c}) = \left(Q^2\left(\frac{m_b}{m_b + m_c}\right)^2 - kEI\right)^2 \geq 0 \quad .$$

Our intermediate conclusions about $\mathrm{F}_2(c^2)$ are: If $k < \frac{4Q^2}{EI}$, $\mathrm{F}_2(c^2)$ will be both negative and positive on $\left(0, \frac{Q}{m_b + m_c}\right)$. If $k > \frac{4Q^2}{EI}$, the values of $\mathrm{F}_2(c^2)$ at both endpoints of the domain will be positive. We have not yet considered any intermediate values.

After simplification, (3.7) gives

$$(3.9) \quad \mathrm{F}_2(c^2) = \left((Q - m_c c^2)m_b c^2 + kEI\right)^2 - 4(Q - m_c c^2)^2 kEI$$

To expedite our analysis, we will introduce a new function, $\mathrm{F}_3(c^2)$. Note that both the first and second terms of (3.9) are squares of positive numbers. Recall that for $a>0$ and $b>0$, $a^2 - b^2 > 0 \Leftrightarrow a > b$. By applying this relationship to (3.9) we get a function with sign identical to $\mathrm{F}_2(c^2)$ for all values of c^2 in $\left(0, \frac{Q}{m_b + m_c}\right)$,

$$(3.10) \quad \begin{cases} \mathrm{F}_3(c^2) = (Q - m_c c^2)m_b c^2 + kEI - 2\sqrt{kEI}\left(Q - m_c c^2\right) \\ \qquad = -m_b m_c c^4 + \left(Qm_b + 2\sqrt{kEI}\, m_c\right)c^2 + \left(kEI - 2Q\sqrt{kEI}\right) \end{cases}.$$

3.4 Analysis of $\mathrm{F}_3(c^2)$.

The graph of $\mathrm{F}_3(c^2)$ is a parabola in c^2 concave downward. Since $\mathrm{F}_2(\frac{Q}{m_b+m_c}) \geq 0$, we have $\mathrm{F}_3(\frac{Q}{m_b+m_c}) > 0$. $\mathrm{F}_3(0)$ may be positive or negative depending on the value of k. Thus, there is at most one zero of $\mathrm{F}_3(c^2)$ on $\left(0, \frac{Q}{m_b+m_c}\right)$. So, $\mathrm{F}_2(c^2) > 0$ on $\left(0, \frac{Q}{m_b+m_c}\right)$ if $k > \frac{4Q^2}{EI}$ and $\mathrm{F}_2(c^2)$ has a zero on $\left(0, \frac{Q}{m_b+m_c}\right)$ if $0<k<\frac{4Q^2}{EI}$.

3.5 Case 1 Solutions.

By substitution of (3.6) and (3.7) into (3.5)

$$(3.11) \quad \lambda^2 = \frac{\mathrm{F}_1(c^2) \pm \sqrt{\mathrm{F}_2(c^2)}}{2(Q-m_c c^2)EI}.$$

$\mathrm{F}_1(c^2)$ is always positive on $\left(0, \frac{Q}{m_b+m_c}\right)$, as is $2(Q-m_c c^2)EI$. For a given value of c, there are two cases for $\mathrm{F}_2(c^2)$,

$$(3.12) \quad \begin{cases} \text{Case 1.1} & \mathrm{F}_2(c^2) > 0 \\ \text{Case 1.2} & \mathrm{F}_2(c^2) < 0 \end{cases}.$$

3.5.1 Solutions for Case 1.1 (Real Eigenvalues).

From the expressions of $\mathrm{F}_1(c^2)$ and $\mathrm{F}_2(c^2)$ at (3.6) and (3.7), $\mathrm{F}_1(c^2) \pm \sqrt{\mathrm{F}_2(c^2)}$ >0, so $\lambda^2 > 0$. Thus λ has two distinct positive roots, and two distinct negative roots. The boundary conditions of the problem ($\lim_{s\to\pm\infty} \hat{z}(s) = \lim_{s\to\pm\infty} \hat{y}(s) = 0$) imply that positive values for λ are not allowed on on $[s_0, \infty]$, where s_0 is the point of transition between Case 1 and Case 2, since such values will cause exponential growth instead of decay for large values of s. Likewise, positive values are required on $[-\infty, -s_0]$. Thus, λ has to take two positive values, say λ_1 and λ_2 on $[-\infty, -s_0]$. This leads to a solution and corresponding derivatives on $[-\infty, -s_0]$

$$(3.13)\quad \begin{cases} \hat{z}(s) = \hat{c}_1 e^{\lambda_1 s} + \hat{c}_2 e^{\lambda_2 s} \\ \hat{z}'(s) = \lambda_1 \hat{c}_1 e^{\lambda_1 s} + \lambda_2 \hat{c}_2 e^{\lambda_2 s} \\ \hat{z}''(s) = \lambda_1^2 \hat{c}_1 e^{\lambda_1 s} + \lambda_2^2 \hat{c}_2 e^{\lambda_2 s} \\ \hat{z}'''(s) = \lambda_1^3 \hat{c}_1 e^{\lambda_1 s} + \lambda_2^3 \hat{c}_2 e^{\lambda_2 s} \end{cases}$$

We translate $s = -s_0$ to the origin by substituting $s - s_0$ for s to get

$$\begin{aligned} \hat{z}(s) &= \hat{c}_1 e^{\lambda_1 (s-s_0)} + \hat{c}_2 e^{\lambda_2 (s-s_0)} \\ \hat{z}'(s) &= \lambda_1 \hat{c}_1 e^{\lambda_1 (s-s_0)} + \lambda_2 \hat{c}_2 e^{\lambda_2 (s-s_0)} \\ \hat{z}''(s) &= \lambda_1^2 \hat{c}_1 e^{\lambda_1 (s-s_0)} + \lambda_2^2 \hat{c}_2 e^{\lambda_2 (s-s_0)} \\ \hat{z}'''(s) &= \lambda_1^3 \hat{c}_1 e^{\lambda_1 (s-s_0)} + \lambda_2^3 \hat{c}_2 e^{\lambda_2 (s-s_0)} \end{aligned}$$

Let $\hat{c}_1 e^{-\lambda_1 s_0} = \tilde{c}_1$ and $\hat{c}_2 e^{-\lambda_2 s_0} = \tilde{c}_2$, to obtain on $[-\infty, 0]$

$$(3.14)\quad \begin{cases} \hat{z}(s) = \tilde{c}_1 e^{\lambda_1 s} + \tilde{c}_2 e^{\lambda_2 s} \\ \hat{z}'(s) = \lambda_1 \tilde{c}_1 e^{\lambda_1 s} + \lambda_2 \tilde{c}_2 e^{\lambda_2 s} \\ \hat{z}''(s) = \lambda_1^{\,2} \tilde{c}_1 e^{\lambda_1 s} + \lambda_2^{\,2} \tilde{c}_2 e^{\lambda_2 s} \\ \hat{z}'''(s) = \lambda_1^{\,3} \tilde{c}_1 e^{\lambda_1 s} + \lambda_2^{\,3} \tilde{c}_2 e^{\lambda_2 s} \end{cases}.$$

3.5.2 Solutions for Case 1.2 (Complex Eigenvalues).

If $F_2(c^2)$ is negative, the values of λ^2 are complex conjugates with positive real parts. Thus there are four possible values for λ: two have positive real parts, and two have negative real parts. Following the same reasoning as Case 1.1 above, the positive-real-part solutions should be excluded on $[s_0, \infty]$, and the negative-real-part solutions should be excluded on $[-\infty, -s_0]$. Let $\lambda = \sigma \pm i\tau,\ \sigma > 0$ on $s \le -s_0$, so

$$\hat{z}(s) = e^{\sigma s}\left[c_0 \cos \tau s + c_1 \sin \tau s\right]$$

$$\hat{z}(s) = e^{\sigma s}\sqrt{c_0^{\,2} + c_1^{\,2}}\left[\frac{c_0}{\sqrt{c_0^{\,2} + c_1^{\,2}}}\cos \tau s + \frac{c_1}{\sqrt{c_0^{\,2} + c_1^{\,2}}}\sin \tau s\right]$$

Let $\sqrt{c_0^{\,2} + c_1^{\,2}} = \mu$, and $\nu = \tan^{-1}\left(\frac{c_1}{c_0}\right)$. Then

$$\hat{z}(s) = e^{\sigma s}\mu\left[\cos \nu \cos \tau s + \sin \nu \sin \tau s\right]$$
$$= e^{\sigma s}\mu \cos\left(\tau s - \nu\right)$$
$$= e^{\sigma s}\mu\, \mathrm{Re}\left(\cos\left(\tau s - \nu\right) + i \sin\left(\tau s - \nu\right)\right)$$
$$= \mathrm{Re}\left[\mu e^{\sigma s + i(\tau s - \nu)}\right] = \mathrm{Re}\left[\mu e^{\lambda s - i\nu}\right]$$

Now let $\lambda = \sigma + i\tau = |\lambda| e^{i\rho}$, where $|\lambda| = \sqrt{\sigma^2 + \tau^2}$ and $\rho = \tan^{-1}\left(\frac{\tau}{\sigma}\right)$, so on $[-\infty, -s_0]$,

$$(3.15)\quad \begin{cases} \hat{z}(s) = e^{\sigma s}\mu\cos(\tau s - \nu) \\ \hat{z}'(s) = |\lambda| e^{\sigma s}\mu\cos(\tau s - \nu + \rho) \\ \hat{z}''(s) = |\lambda|^2 e^{\sigma s}\mu\cos(\tau s - \nu + 2\rho) \\ \hat{z}'''(s) = |\lambda|^3 e^{\sigma s}\mu\cos(\tau s - \nu + 3\rho) \end{cases}$$

We translate $s = -s_0$ to the origin by substituting $s - s_0$ for s to get

$$\begin{aligned} \hat{z}(s) &= e^{\sigma(s-s_0)}\mu\cos(\tau(s-s_0) - \nu) \\ \hat{z}'(s) &= |\lambda| e^{\sigma(s-s_0)}\mu\cos(\tau(s-s_0) - \nu + \rho) \\ \hat{z}''(s) &= |\lambda|^2 e^{\sigma(s-s_0)}\mu\cos(\tau(s-s_0) - \nu + 2\rho) \\ \hat{z}'''(s) &= |\lambda|^3 e^{\sigma(s-s_0)}\mu\cos(\tau(s-s_0) - \nu + 3\rho) \end{aligned}$$

Let $\hat{\mu} = \mu e^{-\sigma s_0}$, so on $[-\infty, 0]$,

$$(3.16)\quad \begin{cases} \hat{z}(s) = e^{\sigma s}\hat{\mu}\cos(\tau(s-s_0) - \nu) \\ \hat{z}'(s) = |\lambda| e^{\sigma s}\hat{\mu}\cos(\tau(s-s_0) - \nu + \rho) \\ \hat{z}''(s) = |\lambda|^2 e^{\sigma s}\hat{\mu}\cos(\tau(s-s_0) - \nu + 2\rho) \\ \hat{z}'''(s) = |\lambda|^3 e^{\sigma s}\hat{\mu}\cos(\tau(s-s_0) - \nu + 3\rho) \end{cases}.$$

3.6 Case 2 Solutions.

From (3.2), $\frac{EI}{k}\hat{z}^{(4)} + \frac{m_b}{k}c^2\hat{z}'' = 1$. Consider the homogeneous case first, with characteristic equation

$$\frac{EI}{k}\lambda^4 + \frac{m_b}{k}c^2\lambda^2 = 0 \Rightarrow \lambda = 0 \text{ or } \lambda^2 = \frac{-m_b c^2}{EI}.$$

This yields

$$\hat{z}_h = d_1 + d_2 s + d_3 \cos(c\sqrt{\frac{m_b}{EI}}s) + d_4 \sin(c\sqrt{\frac{m_b}{EI}}s).$$

Since the non-homogeneous term is a constant, by the undetermined coefficient method, $\hat{z}_p$, a particular solution, can be expressed as $\hat{z}_p = d_5 s^2$, so $\frac{EI}{k}\hat{z}_p^{(4)} + \frac{m_b}{k}c^2\hat{z}'' = 1$, and $\hat{z}_p'' = 2d_5 = \frac{k}{m_b c^2} \Rightarrow d_5 = \frac{k}{2m_b c^2}$. This gives our solution:

$$\hat{z} = d_1 + d_2 s + \frac{ks^2}{2m_b c^2} + d_3 \cos(c\sqrt{\frac{m_b}{EI}}s) + d_4 \sin(c\sqrt{\frac{m_b}{EI}}s).$$

It is natural to assume that the Case Two solution is even, so $d_2 = d_4 = 0$, and

$\hat{z} = d_1 + \frac{ks^2}{2m_b c^2} + d_3 \cos\left(c\sqrt{\frac{m_b}{EI}}s\right)$. Let $\omega = c\sqrt{\frac{m_b}{EI}}$ to get

(3.17) $\hat{z} = d_1 + \frac{ks^2}{2m_b c^2} + d_3 \cos(\omega s)$ on $[-s_0, s_0]$.

The derivatives of $\hat{z}$ are:

(3.18)
$$\begin{cases} \hat{z}(s) = d_1 + \frac{ks^2}{2m_b c^2} + d_3 \cos(\omega s) \\ \hat{z}'(s) = \frac{ks}{m_b c^2} - d_3 \omega \sin(\omega s) \\ \hat{z}''(s) = \frac{k}{m_b c^2} - d_3 \omega^2 \cos(\omega s) \\ \hat{z}'''(s) = d_3 \omega^3 \sin(\omega s) \end{cases}$$

We translate $s = -s_0$ to the origin by substituting $s - s_0$ for s to get

$$(3.19)\quad \begin{cases} \hat{z}(s) = d_1 + \dfrac{k(s-s_0)^2}{2m_b c^2} + d_3\cos(\omega(s-s_0)) \\ \hat{z}'(s) = \dfrac{k(s-s_0)}{m_b c^2} - d_3\omega\sin(\omega(s-s_0)) \\ \hat{z}''(s) = \dfrac{k}{m_b c^2} - d_3\omega^2\cos(\omega(s-s_0)) \\ \hat{z}'''(s) = d_3\omega^3\sin(\omega(s-s_0)) \end{cases}$$

The domain for s changes from $[-s_0, s_0]$ to $[0, 2s_0]$ after the translation.

3.7 Solutions for $\hat{y}(s)$.

After the translations made above, $\hat{z}(0) - \hat{y}(0) = -1$. Here we calculate $\hat{y}(s)$ by using (2.9). $\hat{y}(s)$ for Case 1.1 is given by

$$(3.20)\quad \hat{y}(s) = \frac{-m_b c^2\left(\tilde{c}_1 e^{\lambda_1 s} + \tilde{c}_2 e^{\lambda_2 s}\right) - EI\left(\lambda_1{}^2\tilde{c}_1 e^{\lambda_1 s} + \lambda_2{}^2\tilde{c}_2 e^{\lambda_2 s}\right)}{(m_c c^2 - Q)}.$$

$\hat{y}(s)$ for Case 1.2 is given by

$$(3.21)\quad \hat{y} = \frac{-m_b c^2 e^{\sigma s}\hat{\mu}\cos\left(\tau(s-s_0) - \nu\right) - EI\,|\,\lambda\,|^2\; e^{\sigma s}\hat{\mu}\cos\left(\tau(s-s_0) - \nu + 2\rho\right)}{(m_c c^2 - Q)}.$$

$\hat{y}(s)$ for Case 2 is given by

$$(3.22)\quad \hat{y} = \frac{-d_1 m_b c^2 - \dfrac{k(s-s_0)^2}{2} - \dfrac{kEI}{m_b c^2}}{(m_c c^2 - Q)}.$$

3.8 Matching Case 1.1 and Case 2 Solutions.

Apply (3.14), (3.19), (3.20), and (3.22) to $\hat{z}(0)-\hat{y}(0)=-1$ and match corresponding derivatives at $s=0$ to obtain

(3.23.1) $$\left(\frac{(m_b+m_c)c^2-Q}{(m_c c^2-Q)}\right)d_1+d_3\cos(\omega s_0)+\frac{((m_b+m_c)c^2-Q)k{s_0}^2+2kEI}{2(m_c c^2-Q)m_b c^2}=-1$$

(3.23.2) $$d_1+\frac{k{s_0}^2}{2m_b c^2}+d_3\cos(\omega s_0)=\tilde{c}_1+\tilde{c}_2$$

(3.23.3) $$-\frac{ks_0}{m_b c^2}+d_3\omega\sin(\omega s_0)=\lambda_1\tilde{c}_1+\lambda_2\tilde{c}_2$$

(3.23.4) $$\frac{k}{m_b c^2}-d_3\omega^2\cos(\omega s_0)=\lambda_1^2\tilde{c}_1+\lambda_2^2\tilde{c}_2$$

(3.23.5) $$-d_3\omega^3\sin(\omega s_0)=\lambda_1^3\tilde{c}_1+\lambda_2^3\tilde{c}_2$$

At this point, we have the five equations above, and five unknowns ($\tilde{c}_1$, $\tilde{c}_2$, d_1, d_3, and s_0). Our next goal is to express $\tilde{c}_1$, $\tilde{c}_2$, d_1, and d_3 in terms of s_0, so that after finding a suitable value for s_0, we will be able to evaluate $\tilde{c}_1$, $\tilde{c}_2$, d_1, and d_3.

An additional factor of λ_1 applied to $(3.23.3)$ gives

$$-\frac{k\lambda_1 s_0}{m_b c^2}+d_3\omega\lambda_1\sin(\omega s_0)=\lambda_1^2\tilde{c}_1+\lambda_1\lambda_2\tilde{c}_2$$

Subtract from $(3.23.4)$ to get

$$\frac{k(1+\lambda_1 s_0)}{m_b c^2}-d_3\omega(\lambda_1\sin(\omega s_0)+\omega\cos(\omega s_0))=\lambda_2(\lambda_2-\lambda_1)\tilde{c}_2.$$

Similarly, an additional factor of λ_1 applied to $(3.23.4)$ gives

$$\frac{k\lambda_1}{m_b c^2}-d_3\lambda_1\omega^2\cos(\omega s_0)=\lambda_1^3\tilde{c}_1+\lambda_1\lambda_2^2\tilde{c}_2.$$

We combine with $(3.23.5)$ by subtraction to get

$$\frac{k\lambda_1}{m_b c^2} - d_3\omega^2(\lambda_1\cos(\omega s_0)\text{-}\omega\sin(\omega s_0)) = (\lambda_1 - \lambda_2)\lambda_2{}^2\tilde{c}_2$$

Add the two resultant equations above and simplify to get

$$d_3(s_0) = \frac{k(\lambda_1 + \lambda_2(1+\lambda_1 s_0))}{m_b c^2\omega((\lambda_1\lambda_2\text{-}\omega^2)\sin(\omega s_0) + \omega(\lambda_2 + \lambda_1)\cos(\omega s_0))}.$$

Our previous combination of $(3.23.4)$ and $(3.23.5)$ above gives

$$\tilde{c}_2(d_3, s_0) = \tilde{c}_2(s_0) = \frac{1}{(\lambda_1 - \lambda_2)\lambda_2{}^2}\left(\frac{k\lambda_1}{m_b c^2} - d_3\omega^2(\lambda_1\cos(\omega s_0)\text{-}\omega\sin(\omega s_0))\right).$$

Similarly we apply an additional factor of , λ_2 to $(3.23.4)$ and combine with $(3.23.5)$ by subtraction to get

$$\tilde{c}_1(d_3, s_0) = \tilde{c}_1(s_0) = \frac{1}{(\lambda_2 - \lambda_1)\lambda_1{}^2}\left(\frac{k\lambda_2}{m_b c^2} - d_3\omega^2(\lambda_2\cos(\omega s_0)\text{-}\omega\sin(\omega s_0))\right).$$

From $(3.23.2)$,

$$d_1(\tilde{c}_1, \tilde{c}_2, d_3, s_0) = d_1(s_0) = \tilde{c}_1 + \tilde{c}_2 - \frac{k{s_0}^2}{2m_b c^2} - d_3\cos(\omega s_0).$$

The last variable is s_0. We will solve numerically from $(3.23.1)$ by finding zeros of $g(s_0)$ defined as

$$g(s_0) = \left(\frac{(m_b + m_c)c^2 - Q}{(m_c c^2 - Q)}\right)d_1 + d_3\cos(\omega s_0) + \frac{((m_b + m_c)c^2 - Q)k{s_0}^2 + 2kEI}{2(m_c c^2 - Q)m_b c^2} + 1 = 0 \ .$$

This gives us the following five equations:

$$(3.24)\begin{cases} g(s_0)=\left(\dfrac{(m_b+m_c)c^2-Q}{(m_c c^2-Q)}\right)d_1+d_3\cos(\omega s_0)+\dfrac{((m_b+m_c)c^2-Q)k{s_0}^2+2kEI}{2(m_c c^2-Q)m_b c^2}+1=0 \\ d_3(s_0)=\dfrac{k\left(\lambda_1+\lambda_2\left(1+\lambda_1 s_0\right)\right)}{m_b c^2\omega\left(\left(\lambda_1\lambda_2-\omega^2\right)\sin(\omega s_0)+\omega(\lambda_2+\lambda_1)\cos(\omega s_0)\right)} \\ \tilde{c}_1(d_3,s_0)=\tilde{c}_1(s_0)=\dfrac{1}{\left(\lambda_2-\lambda_1\right){\lambda_1}^2}\left(\dfrac{k\lambda_2}{m_b c^2}-d_3\omega^2(\lambda_2\cos(\omega s_0)-\omega\sin(\omega s_0))\right) \\ \tilde{c}_2(d_3,s_0)=\tilde{c}_2(s_0)=\dfrac{1}{\left(\lambda_1-\lambda_2\right){\lambda_2}^2}\left(\dfrac{k\lambda_1}{m_b c^2}-d_3\omega^2(\lambda_1\cos(\omega s_0)-\omega\sin(\omega s_0))\right) \\ d_1(\tilde{c}_1,\tilde{c}_2,d_3,s_0)=d_1(s_0)=\tilde{c}_1+\tilde{c}_2-\dfrac{k{s_0}^2}{2m_b c^2}-d_3\cos(\omega s_0) \end{cases}$$

At this point, we need to revisit the functions that describe the position of the roadbed and cable. For the roadbed,

$$(3.25)\begin{cases} \hat{z}(s)=\tilde{c}_1 e^{\lambda_1 s}+\tilde{c}_2 e^{\lambda_2 s} & \text{for } s<0 \\ \hat{z}(s)=d_1+\dfrac{k(s-s_0)^2}{2m_b c^2}+d_3\cos(\omega(s-s_0)) & \text{for } 0<s<2s_0 \\ \hat{z}(s)=\hat{z}(-s+2s_0) & \text{for } s>2s_0 \end{cases}.$$

For the supporting cable,

$$(3.26)\begin{cases} \hat{y}(s)=\dfrac{-m_b c^2\left(\tilde{c}_1 e^{\lambda_1 s}+\tilde{c}_2 e^{\lambda_2 s}\right)-EI\left({\lambda_1}^2\tilde{c}_1 e^{\lambda_1 s}+{\lambda_2}^2\tilde{c}_2 e^{\lambda_2 s}\right)}{(m_c c^2-Q)} & \text{for } s<0 \\ \hat{y}(s)=\dfrac{-d_1 m_b c^2-\dfrac{k(s-s_0)^2}{2}-\dfrac{kEI}{m_b c^2}}{(m_c c^2-Q)} & \text{for } 0<s<2s_0 \\ \hat{y}(s)=\hat{y}(-s+2s_0) & \text{for } s>2s_0 \end{cases}$$

3.9 Matching Case 1.2 and Case 2 Solutions.

Apply (3.16), (3.19), (3.21), and (3.22) to $\hat{z}(0) - \hat{y}(0) = -1$, then simplify to get

$$(3.27)\quad \begin{cases} \dfrac{\hat{\mu}}{(m_c c^2 - Q)}\Big(\big((m_b + m_c)c^2 - Q\big)\cos\big(\tau s_0 + \nu\big) + EI \mid \lambda \mid^2 \cos\big(\tau s_0 + \nu - 2\rho\big)\Big) = -1 \\ \left(\dfrac{(m_b + m_c)c^2 - Q}{(m_c c^2 - Q)}\right) d_1 + d_3 \cos(\omega s_0) + \dfrac{\big((m_b + m_c)c^2 - Q\big)k{s_0}^2 + 2kEI}{2(m_c c^2 - Q)m_b c^2} = -1 \end{cases}$$

The first three derivatives also match at $s = 0$, so

$$(3.28)\quad \begin{cases} \hat{z}(0) = d_1 + \dfrac{k{s_0}^2}{2m_b c^2} + d_3 \cos(\omega s_0) = \hat{\mu}\cos\big(\tau s_0 + \nu\big) \\ \hat{z}'(0) = \dfrac{-ks_0}{m_b c^2} + d_3 \omega \sin(\omega s_0) = \mid \lambda \mid \hat{\mu}\cos\big(\tau s_0 + \nu - \rho\big) \\ \hat{z}''(0) = \dfrac{k}{m_b c^2} - d_3 \omega^2 \cos(\omega s_0) = \mid \lambda \mid^2 \hat{\mu}\cos\big(\tau s_0 + \nu - 2\rho\big) \\ \hat{z}'''(0) = -d_3 \omega^3 \sin(\omega s_0) = \mid \lambda \mid^3 \hat{\mu}\cos\big(\tau s_0 + \nu - 3\rho\big) \end{cases}.$$

This gives us five equations to solve for five unknowns:

$$(3.29.1)\quad d_1 + \frac{k{s_0}^2}{2m_b c^2} + d_3 \cos(\omega s_0) = \hat{\mu}\cos\big(\tau s_0 + \nu\big)$$

$$(3.29.2)\quad \left(\frac{(m_b + m_c)c^2 - Q}{(m_c c^2 - Q)}\right) d_1 + d_3 \cos(\omega s_0) + \frac{\big((m_b + m_c)c^2 - Q\big)k{s_0}^2 + 2kEI}{2(m_c c^2 - Q)m_b c^2} = -1$$

$$(3.29.3)\quad \frac{-ks_0}{m_b c^2} + d_3 \omega \sin(\omega s_0) = \mid \lambda \mid \hat{\mu}\cos\big(\tau s_0 + \nu - \rho\big)$$

$$(3.29.4)\quad \frac{k}{m_b c^2} - d_3 \omega^2 \cos(\omega s_0) = \mid \lambda \mid^2 \hat{\mu}\cos\big(\tau s_0 + \nu - 2\rho\big)$$

$$(3.29.5)\quad -d_3 \omega^3 \sin(\omega s_0) = \mid \lambda \mid^3 \hat{\mu}\cos\big(\tau s_0 + \nu - 3\rho\big)$$

Note that the expression $\tau s_0 + \nu$ is present every time ν appears. Let $\gamma = \tau s_0 + \nu$, which gives

$$
\begin{cases}
(3.30.1) \quad d_1 + \dfrac{ks_0{}^2}{2m_bc^2} + d_3\cos(\omega s_0) = \hat{\mu}\cos(\gamma) \\
(3.30.2) \quad \left(\dfrac{(m_b+m_c)c^2 - Q}{(m_cc^2 - Q)}\right)d_1 + d_3\cos(\omega s_0) + \dfrac{((m_b+m_c)c^2 - Q)ks_0{}^2 + 2kEI}{2(m_cc^2 - Q)m_bc^2} = -1 \\
(3.30.3) \quad \dfrac{-ks_0}{m_bc^2} + d_3\omega\sin(\omega s_0) = |\lambda|\hat{\mu}\cos(\gamma - \rho) \\
(3.30.4) \quad \dfrac{k}{m_bc^2} - d_3\omega^2\cos(\omega s_0) = |\lambda|^2\ \hat{\mu}\cos(\gamma - 2\rho) \\
(3.30.5) \quad -d_3\omega^3\sin(\omega s_0) = |\lambda|^3\ \hat{\mu}\cos(\gamma - 3\rho)
\end{cases}
$$

As seen previously, we have the five equations above, and five unknowns (d_1, d_3, s_0, $\hat{\mu}$, and γ). Also as before, the next step is to express d_1, d_3, s_0, and $\hat{\mu}$ in terms of γ, so that after finding a suitable value for γ, we will be able to evaluate d_1, d_3, s_0, and $\hat{\mu}$.

We note that the first equation in (3.27) is equivalent to the information in our five equations, and is convenient, in that it gives us the following relationship after simple manipulation.

$$\hat{\mu}(\gamma) = \frac{-(m_cc^2 - Q)}{\left(\left((m_b+m_c)c^2 - Q\right)\cos(\gamma) + EI|\lambda|^2\cos(\gamma - 2\rho)\right)}.$$

To solve for s_0, consider $(3.30.3)$ and $(3.30.5)$. Rearrange to

$$
\begin{aligned}
d_3\sin(\omega s_0) &= \frac{1}{\omega}\left(|\lambda|\hat{\mu}\cos(\gamma - \rho) + \frac{ks_0}{m_bc^2}\right). \\
-d_3\sin(\omega s_0) &= \frac{1}{\omega^3}|\lambda|^3\ \hat{\mu}\cos(\gamma - 3\rho)
\end{aligned}
$$

Sum the equations, then rearrange to get

$$s_0(\hat{\mu}, \gamma) = -\frac{\hat{\mu}|\lambda|m_bc^2}{k}\cos(\gamma - \rho) - \frac{EI\hat{\mu}}{k}|\lambda|^3\cos(\gamma - 3\rho).$$

We get $d_1(d_3, s_0, \hat{\mu}, \gamma)$ directly from (3.30.1),

$$d_1(d_3, s_0, \hat{\mu}, \gamma) = -\frac{k{s_0}^2}{2m_b c^2} - d_3 \cos(\omega s_0) + \hat{\mu}\cos(\gamma).$$

From (3.30.5),

$$d_3(\gamma, s_0, \hat{\mu}) = -\frac{|\lambda|^3\ \hat{\mu}\cos(\gamma - 3\rho)}{\omega^3 \sin(\omega s_0)}.$$

The last of the unknowns is γ. We solve from (3.30.4) by defining a new function, and looking numerically for the zeros. Our function is

$$f(d_3, s_0, \hat{\mu}, \gamma) = f(\gamma) = \frac{k}{\hat{\mu} m_b c^2} - \frac{d_3 \omega^2 \cos(\omega s_0)}{\hat{\mu}} - |\lambda|^2\ \cos(\gamma - 2\rho).$$

We now have the following equations that allow us to evaluate our functions.

$$(3.31)\quad \begin{cases} f(d_3, s_0, \hat{\mu}, \gamma) = f(\gamma) = \dfrac{k}{\hat{\mu} m_b c^2} - \dfrac{d_3 \omega^2 \cos(\omega s_0)}{\hat{\mu}} - |\lambda|^2\ \cos(\gamma - 2\rho) = 0 \\ \hat{\mu}(\gamma) = \dfrac{-(m_c c^2 - Q)}{\left(\left((m_b + m_c)c^2 - Q\right)\cos(\gamma) + EI\,|\lambda|^2\ \cos(\gamma - 2\rho)\right)} \\ s_0(\hat{\mu}, \gamma) = s_0(\gamma) = -\dfrac{\hat{\mu}\,|\lambda|\, m_b c^2}{k}\cos(\gamma - \rho) - \dfrac{EI\,\hat{\mu}}{k}|\lambda|^3\ \cos(\gamma - 3\rho) \\ d_3(\gamma, s_0) = d_3(\gamma) = -\dfrac{|\lambda|^3\ \hat{\mu}\cos(\gamma - 3\rho)}{\omega^3 \sin(\omega s_0)} \\ d_1(d_3, s_0, \hat{\mu}, \gamma) = d_1(\gamma) = -\dfrac{k{s_0}^2}{2m_b c^2} - d_3 \cos(\omega s_0) + \hat{\mu}\cos(\gamma) \end{cases}$$

As in the previous case, it is time to reconsider the equations for the position of the roadbed and support cable. Recall the description of the roadbed

$$(3.32)\quad \begin{cases} \hat{z}(s) = e^{\sigma s}\hat{\mu}\cos(\tau(s - s_0) - \nu) = e^{s\,\mathrm{Re}(\lambda)}\hat{\mu}\cos(s\,\mathrm{Im}(\lambda) - \gamma) = \hat{z}(s, \gamma) & \text{for } s < 0 \\ \hat{z}(s) = d_1 + \dfrac{k(s - s_0)^2}{2m_b c^2} + d_3 \cos(\omega(s - s_0)) = \hat{z}(s, \gamma) & \text{for } 0 < s < 2s_0 \\ \hat{z}(s) = \hat{z}(-s + 2s_0) & \text{for } s > 2s_0 \end{cases}.$$

And the description of the cable

$$(3.33)\quad \begin{cases} \hat{y}(s) = \dfrac{-m_b c^2 e^{s\,\mathrm{Re}(\lambda)}\hat{\mu}\cos\left(s\,\mathrm{Im}(\lambda)-\gamma\right) - EI\,|\,\lambda\,|^2\; e^{s\,\mathrm{Re}(\lambda)}\hat{\mu}\cos\left(s\,\mathrm{Im}(\lambda)-\gamma+2\rho\right)}{(m_c c^2 - Q)} & \text{for } 0 < s < 2s_0 \\ \hat{y}(s) = \dfrac{-d_1 m_b c^2 - \dfrac{k(s-s_0)^2}{2} - \dfrac{k}{\omega^2}}{(m_c c^2 - Q)} & \text{for } 0 < s < 2s_0 \\ \hat{z}(s) = \hat{z}(-s+2s_0) & \text{for } s > 2s_0 \end{cases}.$$

CHAPTER 4

NUMERICAL COMPUTATIONS

At this point, we change our mode of operations. So far, we have approached the solutions using analytic processes. Now, we will use numerical methods to finalize our solutions. The software we use is MAPLE, a powerful mathematics package designed for use in these kinds of mathematics, physics, and engineering problems.

4.1 Matching Cases 1.1 and 2.

The first steps in this phase of the solution process is to establish values for constants used in the problem. We decided to use the following constants:

$$(4.1)\begin{cases} EI = 16 \\ m_c = 1 \\ m_b = 3 \\ Q = 4 \\ k = 1 \end{cases}$$

The next step is to establish a value for c. From (2.10) we have the upper bound of $c = 1$. We apply the quadratic formula to (3.10) to find the lower bound for c still in Case 1.1. After coding it into the computer, we find the break point between Case 1.1 and Case 1.2 to occur at approximately $c_0 = .9641745088$. Based on these boundaries, we choose $c = .98$, near the center of the feasible interval.

We use the definition at the beginning of Section 3.6 to evaluate $\omega = .4243524480$, and move on to evaluate the eigenvalues for these specifications. After a little fairly direct computer coding we arrive at $\lambda_1 = .1632043211$ and $\lambda_2 = .3496855819$. These are the last preparatory steps needed before we can solve for the variables at (3.24).

We coded the functions from (3.24) for $d_3(s_0)$, $\tilde{c}_1(s_0)$, $\tilde{c}_2(s_0)$, and $d_1(s_0)$. We use these relationships to establish values of $g(s_0)$ (also from (3.24)) and graph these values over a range of s_0 so we can look for zeros of the function. We observe $g(s_0) = 0$ between $s_0 = 5$ and $s_0 = 6$ (See figure 4.1). We use MAPLE to obtain $s_0 = 5.819100173$.

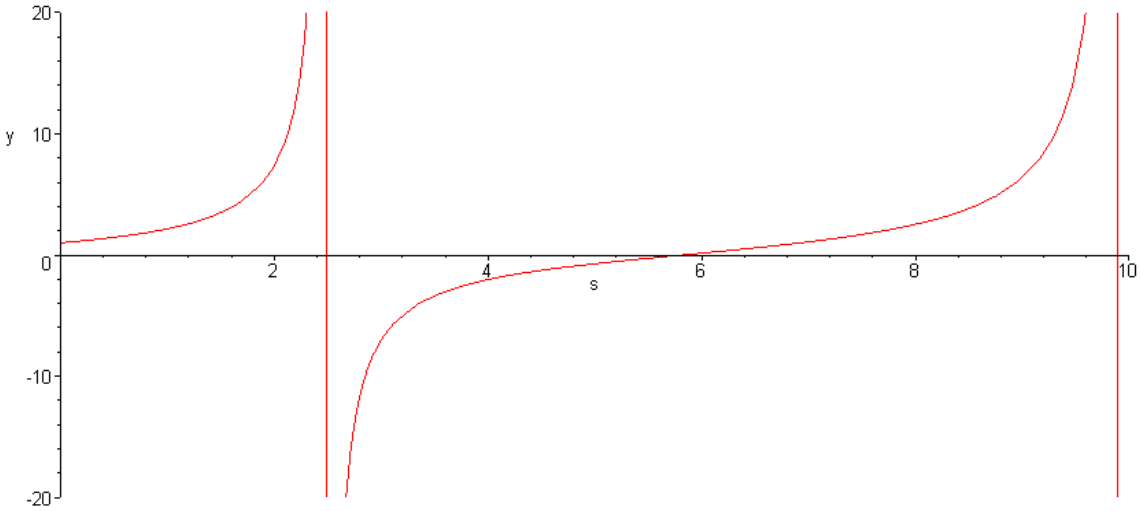

Figure 4.1. $g(s_0)$ for $c = .98$.

This allows us to get numerical values for the functions:

$d_3(s_0)$= -2.799253021
$\tilde{c}_1(s_0)$= -30.15006972
$\tilde{c}_2(s_0)$= 6.180423468
$d_1(s_0)$= -32.03621472

At this point, we have enough information to find and graph $\hat{z}(s)-\hat{y}(s)$. We coded the functions from (3.25) and (3.26) to get a graph that matches at $\hat{z}(0)-\hat{y}(0)=-1$ as expected. After adjusting the functions to center at zero, we obtain the desired graph of $\hat{z}(s)-\hat{y}(s)$ that represents a traveling wave solution of (2.12).

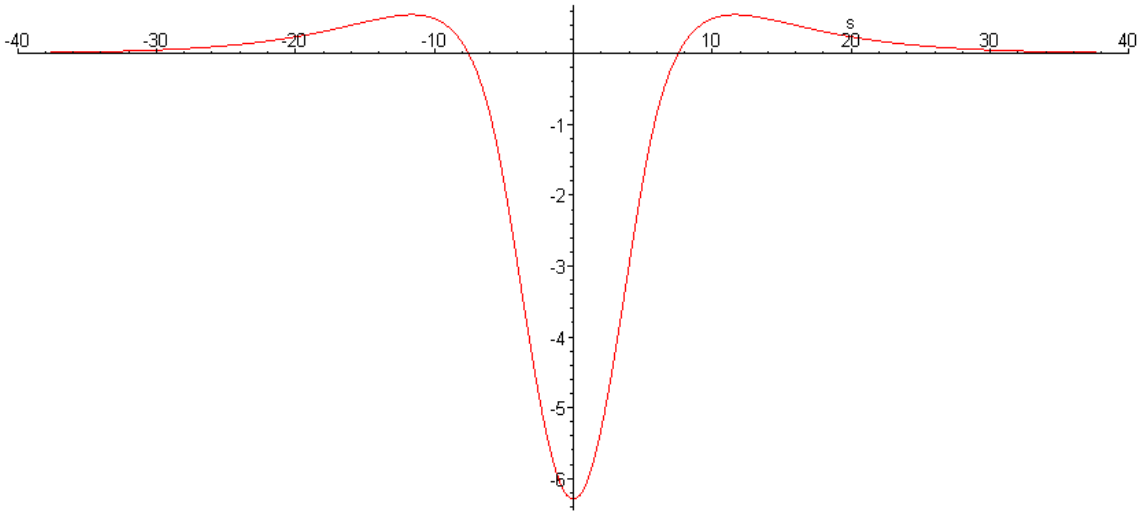

Figure 4.2. $\hat{z}(s)-\hat{y}(s)$ for real eigenvalue case, $c=.98$, $s_0=5.819100173$.

As interesting as the plot for $\hat{z}(s)-\hat{y}(s)$ is, we might be even more interested in the graphs of $\hat{z}(s)$ and $\hat{y}(s)$ individually. Those graphs follow here.

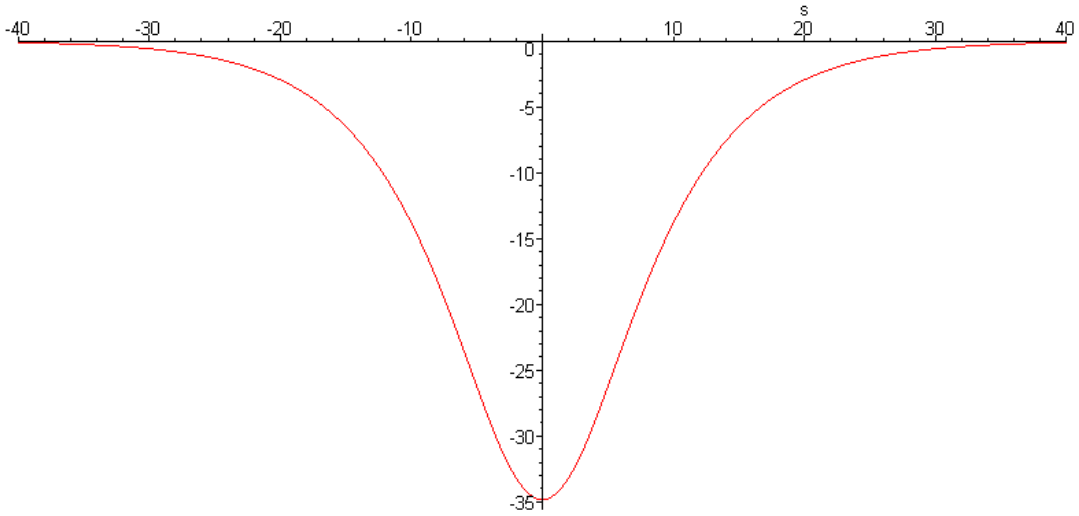

Figure 4.3. $\hat{z}(s)$ for real eigenvalue case, $c = .98$, $s_0 = 5.819100173$.

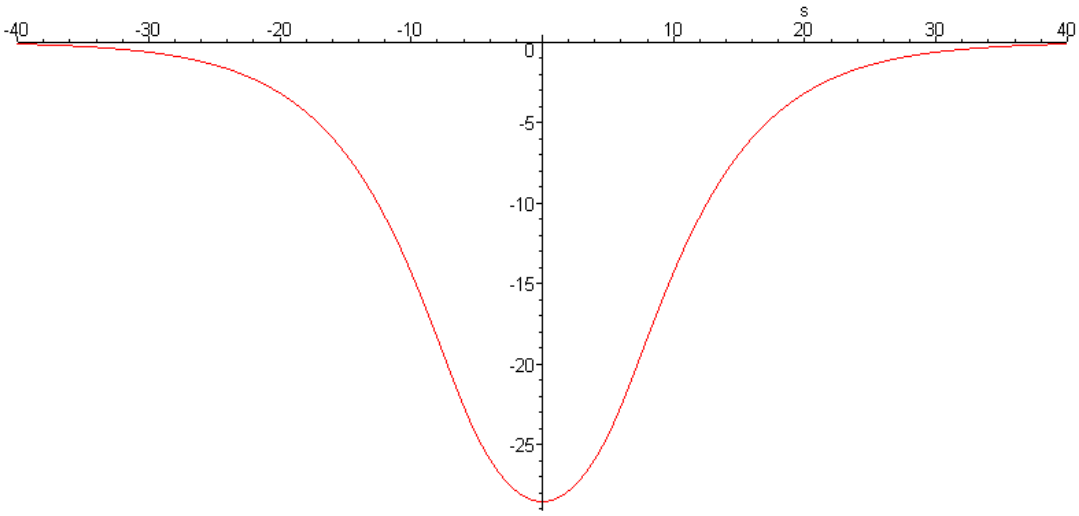

Figure 4.4. . $\hat{y}(s)$ for real eigenvalue case, $c = .98$, $s_0 = 5.819100173$.

Note that the shapes of the two curves are similar to one another, and not entirely unlike their difference. Further, note that the amplitude (movement from the static position) is substantially more than might be suspected from looking at the difference function alone.

By varying the value of c within this case, and using the same programing and methods, we get the following graphs.

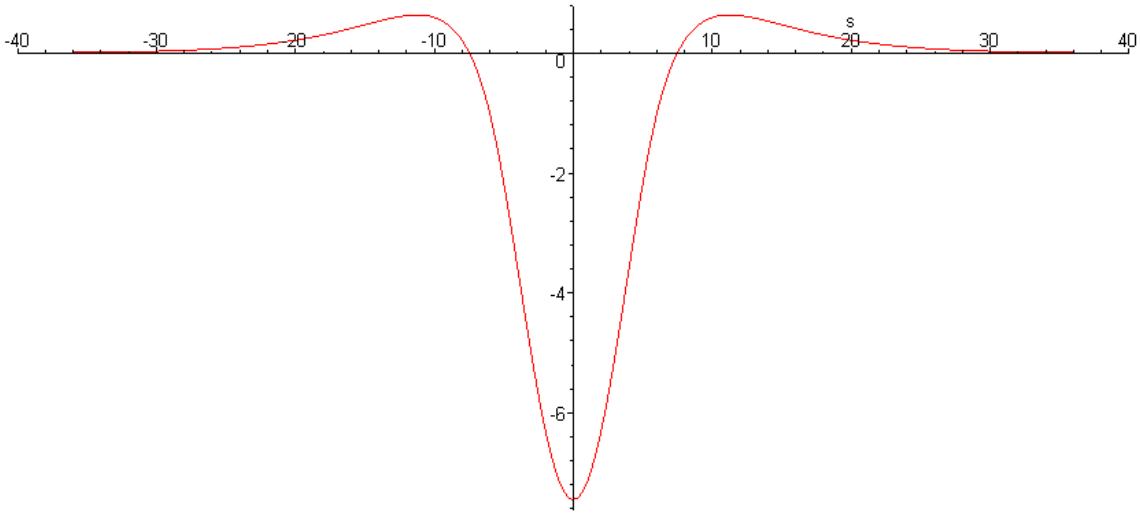

Figure 4.5. $\hat{z}(s) - \hat{y}(s)$ for real eigenvalue case, $c = .97$, $s_0 = 6.019553553$.

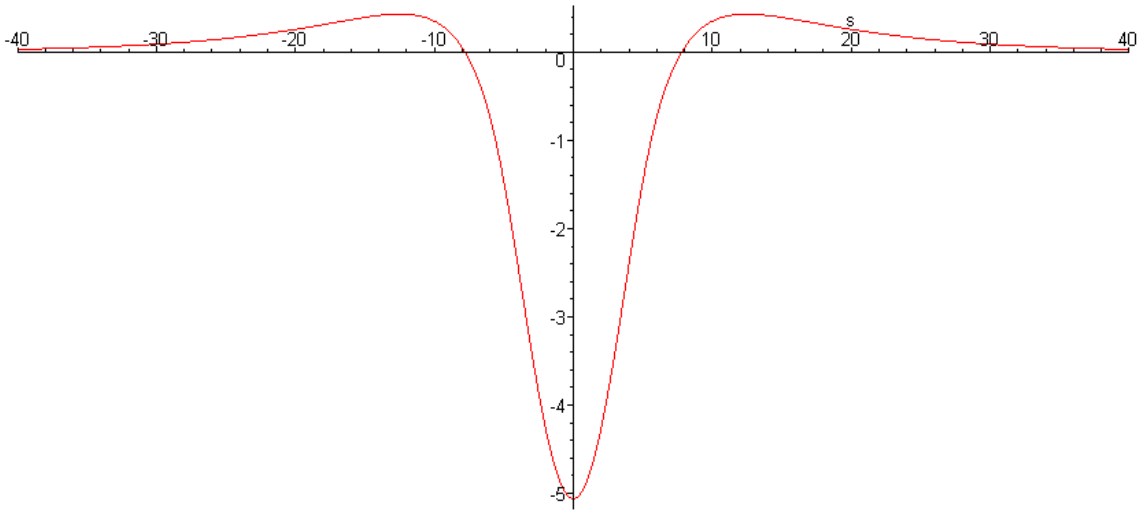

Figure 4.6. $\hat{z}(s) - \hat{y}(s)$ for real eigenvalue case, $c = .99$, $s_0 = 5.594570170$.

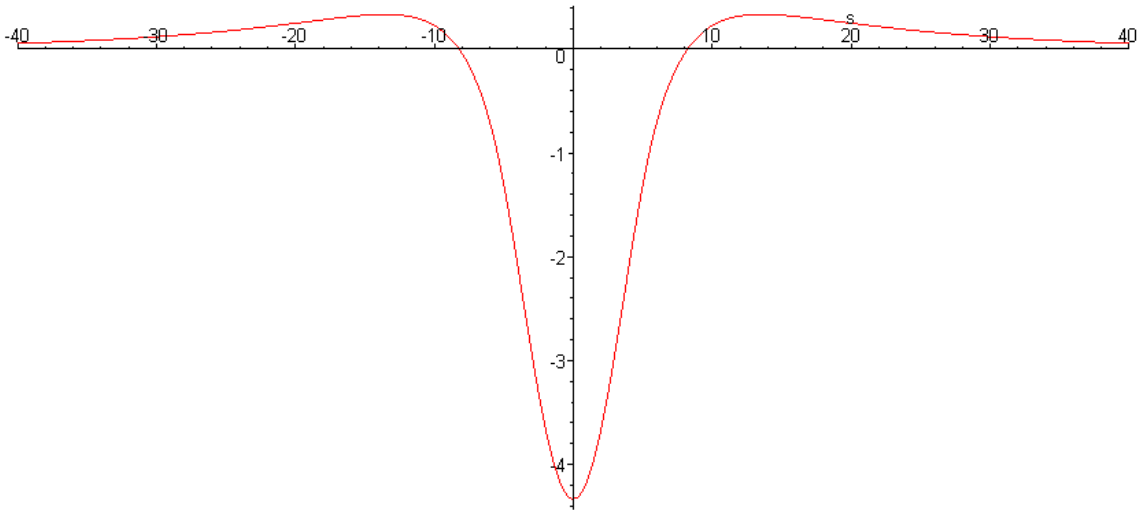

Figure 4.7. $\hat{z}(s) - \hat{y}(s)$ for real eigenvalue case, $c = .995$, $s_0 = 5.464024723$.

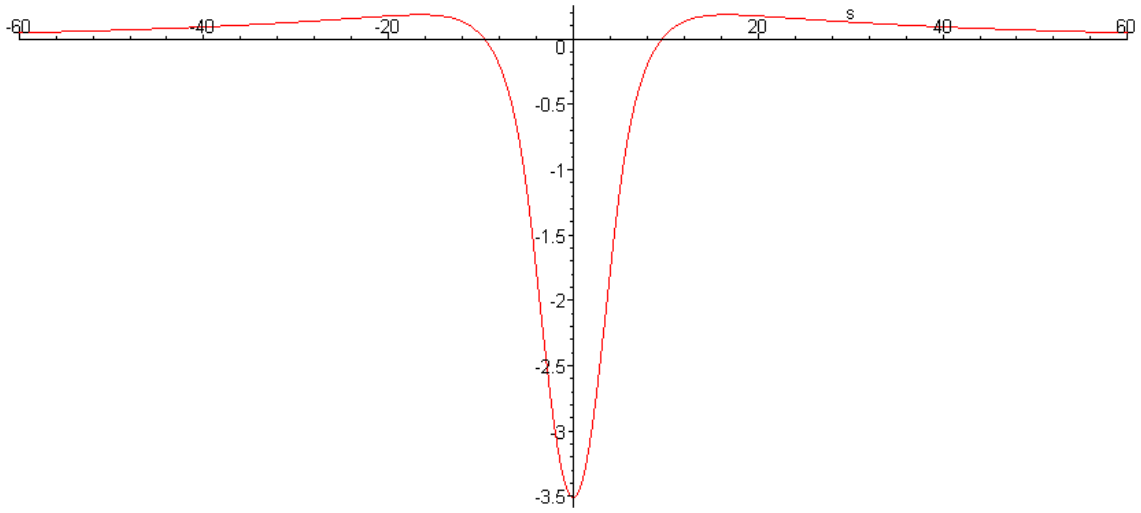

Figure 4.8. $\hat{z}(s) - \hat{y}(s)$ for real eigenvalue case, $c = .999$, $s_0 = 5.337533082$.

We note that the results are very similar for all the values tested. They do vary some in amplitude and width, with the general trend being to get shorter and wider as the wave speed increases. Recall that the maximum wave speed is $c = 1.0$. If we look at the plots of $\hat{z}(s)$ and $\hat{y}(s)$ by themselves for the last case (

$c = .999$), the wider for faster wave speeds part of the above observation becomes significantly more obvious.

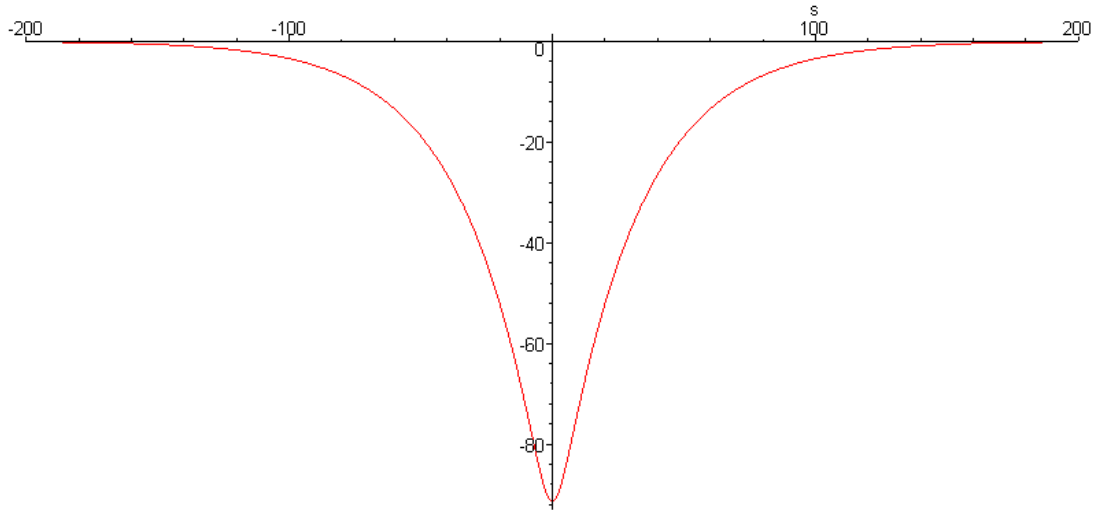

Figure 4.9. $\hat{z}(s)$ for real eigenvalue case, $c = .999$, $s_0 = 5.337533082$.

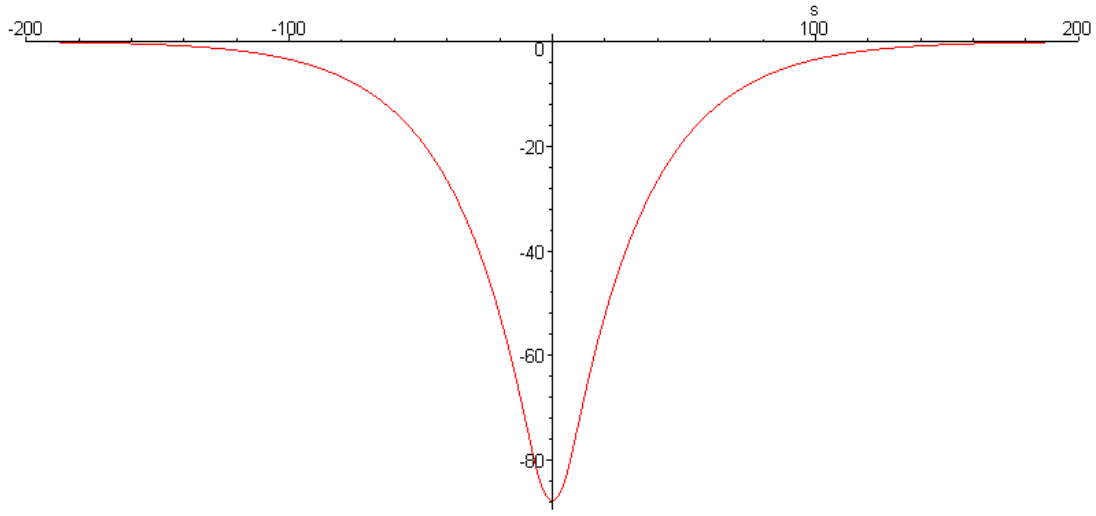

Figure 4.10. $\hat{y}(s)$ for real eigenvalue case, $c = .999$, $s_0 = 5.337533082$.

The height and width of these waves might make it unlikely to observe them on an actual bridge. Hoping for something more interesting, we note that the zeros of $g(s_0)$ repeat with a degree of regularity (Figure 4.11). We select $c = .97$ and choose the second and third zeros of the function using our established method to get the following two graphs (Figures 4.12 and 4.13).

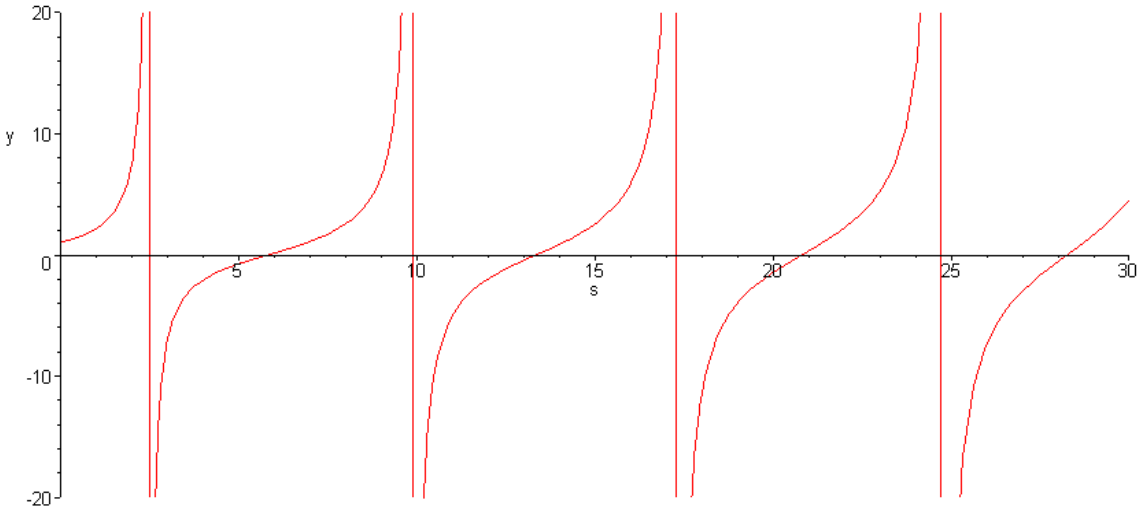

Figure 4.11. $g(s_0)$ (extended scale) for $c = .97$.

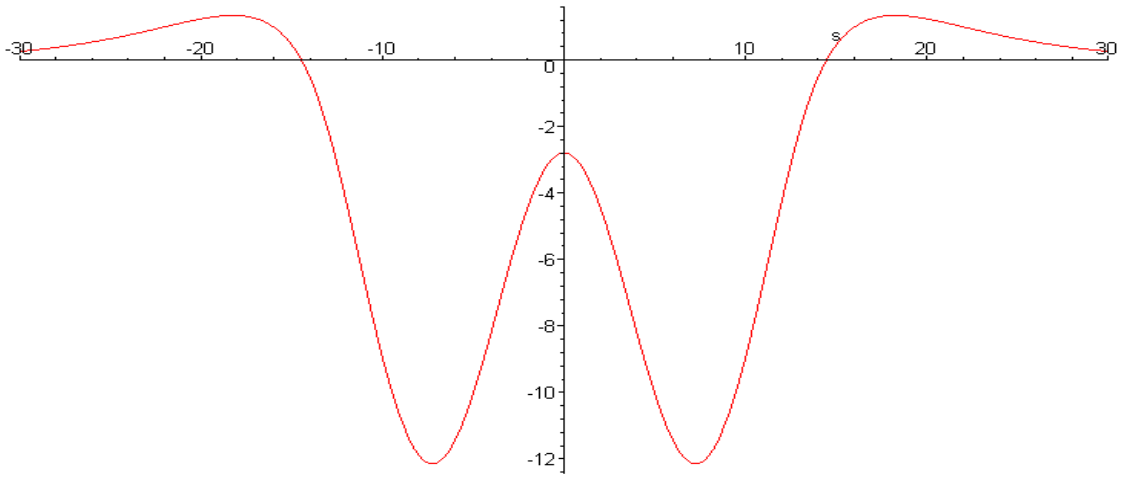

Figure 4.12. $\hat{z}(s) - \hat{y}(s)$ for real eigenvalue case, $c = .97$, $s_0 = 13.64302955$.

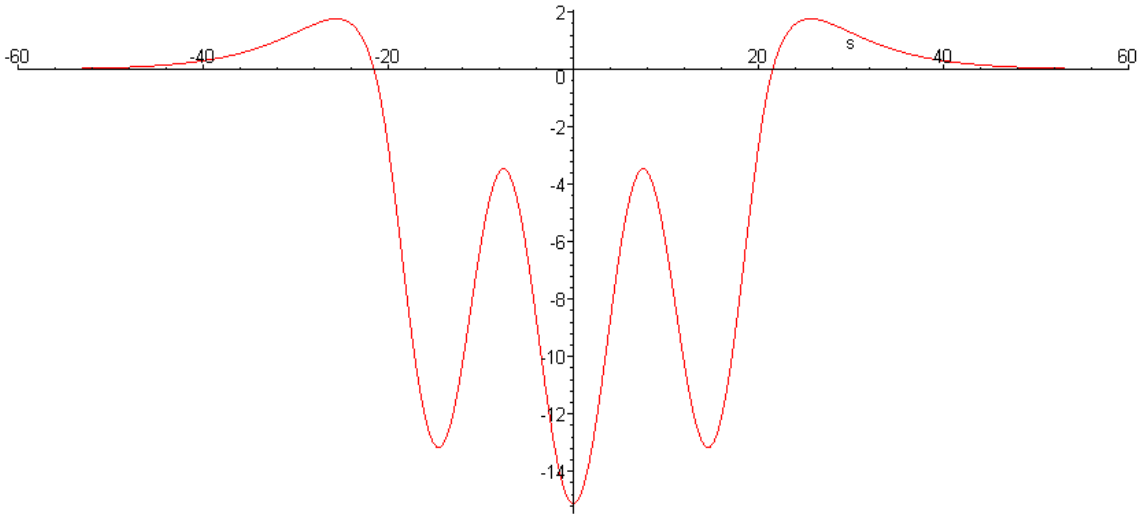

Figure 4.13. $\hat{z}(s) - \hat{y}(s)$ for real eigenvalue case, $c = .97$, $s_0 = 20.81159817$.

We also graph $\hat{z}(s)$ and $\hat{y}(s)$ independently for the same case as graphed in Figure 4.13.

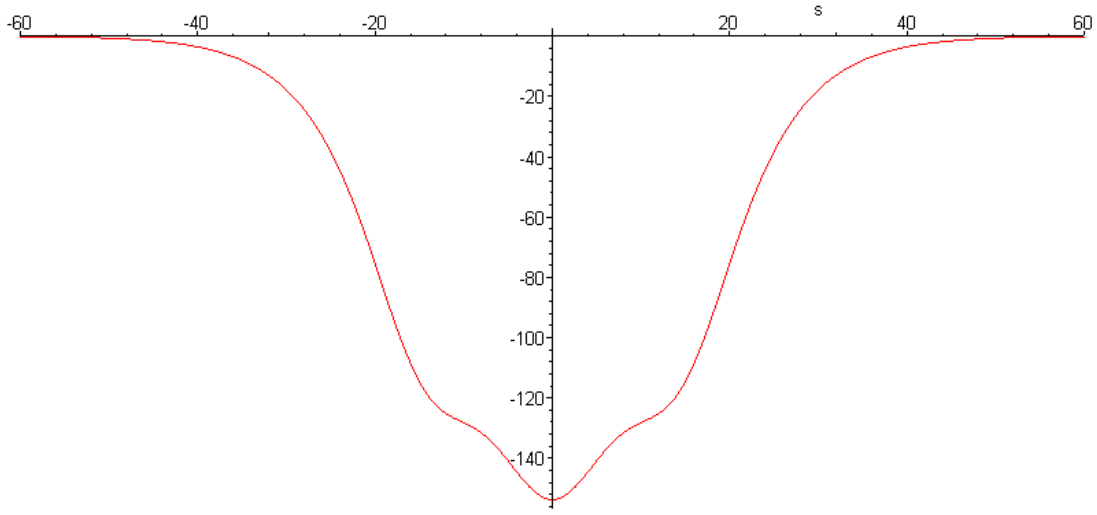

Figure 4.14. $\hat{z}(s)$ for real eigenvalue case, $c = .97$, $s_0 = 20.81159817$.

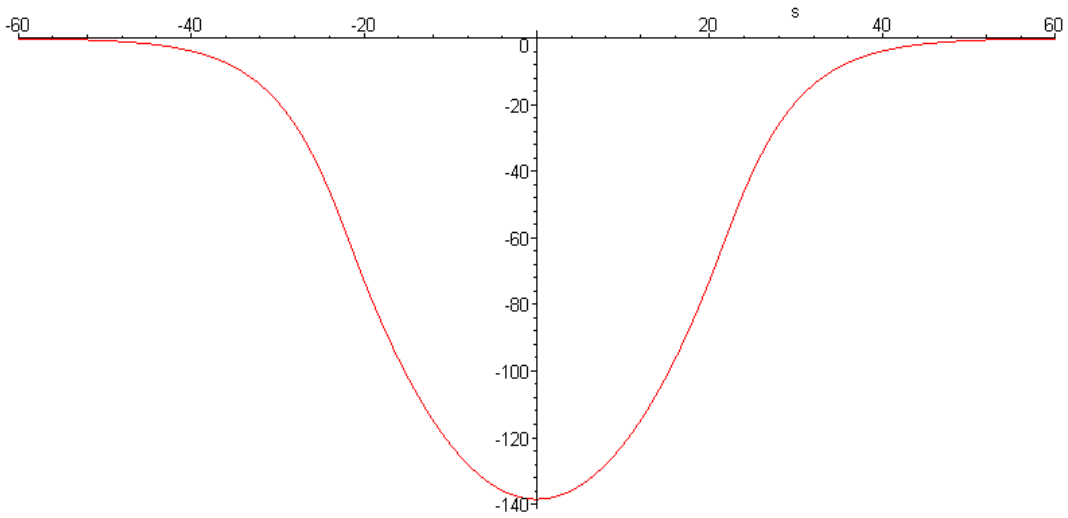

Figure 4.15. $\hat{y}(s)$ for real eigenvalue case, $c = .97$, $s_0 = 20.81159817$.

These solutions are substantially more interesting. The amplitude is greater, and it appears at first glance that if we take the first zero of $g(s_0)$, we get a single peak; if we take the second, two peaks; if we take the third, three. This may be a special case, but is certainly shows promise. Note that the large amplitude and corresponding area under the curve indicates considerable movement from the neutral position. It would certainly take a substantial input of energy to the system to result in these waves. In fact, while they are mathematical solutions to the system, it may be unlikely that any actual bridge could deform to this degree.

4.2 Matching Cases 1.2 and 2.

The methodology here is just about the same as for the real-valued eigenvalue case above. We start with the same constants chosen in (4.1). Based on the analysis in section 4.1 above, we choose $c = .9$ to ensure that we

are within the correct case (complex eigenvalues). After coding the functions from (3.5), (3.6), and (3.7), have $\lambda = .3184556921 - .1435678095i$.

Now we have enough information to solve for $\rho = -.4235398426$ as defined in section 3.5.2. This, in turn, gives us enough information to establish coding for $\hat{\mu}(\gamma)$, $s_0(\gamma)$, $d_3(\gamma)$, and $d_1(\gamma)$. These relationships are used to evaluate and graph $f(\gamma)$ (Figure 4.9). We note a zero of the function at about $\gamma = 3.6$; MAPLE establishes the value $\gamma = 3.609832084$.

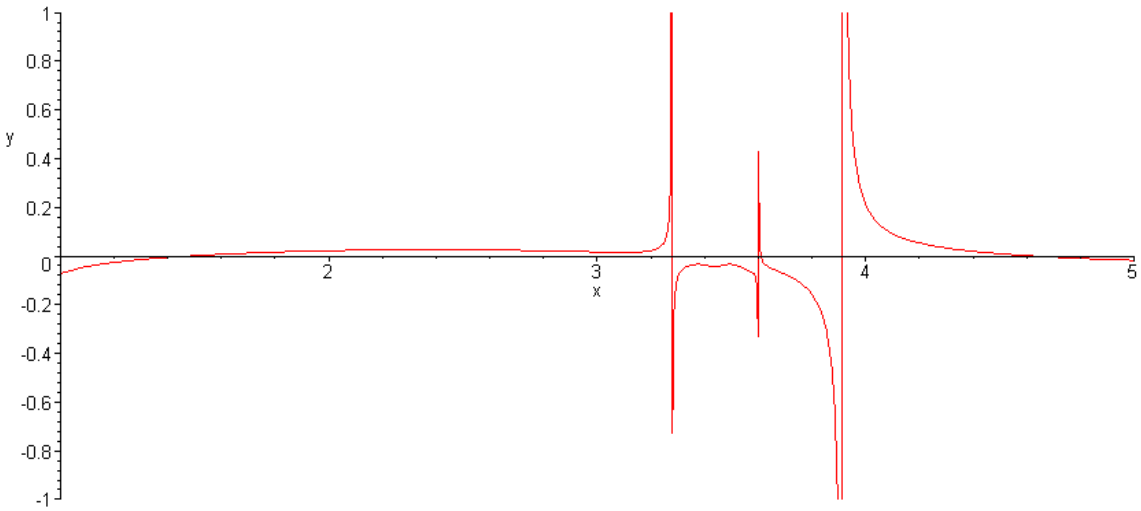

Figure 4.16. $f(\gamma)$ for $c = .9$.

The evaluation of γ allows us to evaluate the functions defined previously:

$$\hat{\mu}(\gamma) = 17.26112399$$
$$s_0(\gamma) = 7.232755051$$
$$d_3(\gamma) = -6.552997055$$
$$d_1(\gamma) = -32.38147104$$

We now have enough information to evaluate and graph the functions at (3.32) and (3.33). We code the functions, graph them, and check that $\hat{z}(0) - \hat{y}(0) = -1$ as expected. As in the previous case, we recenter the functions and plot the representation of $\hat{z}(s) - \hat{y}(s)$, which represents a traveling wave solution to (2.12).

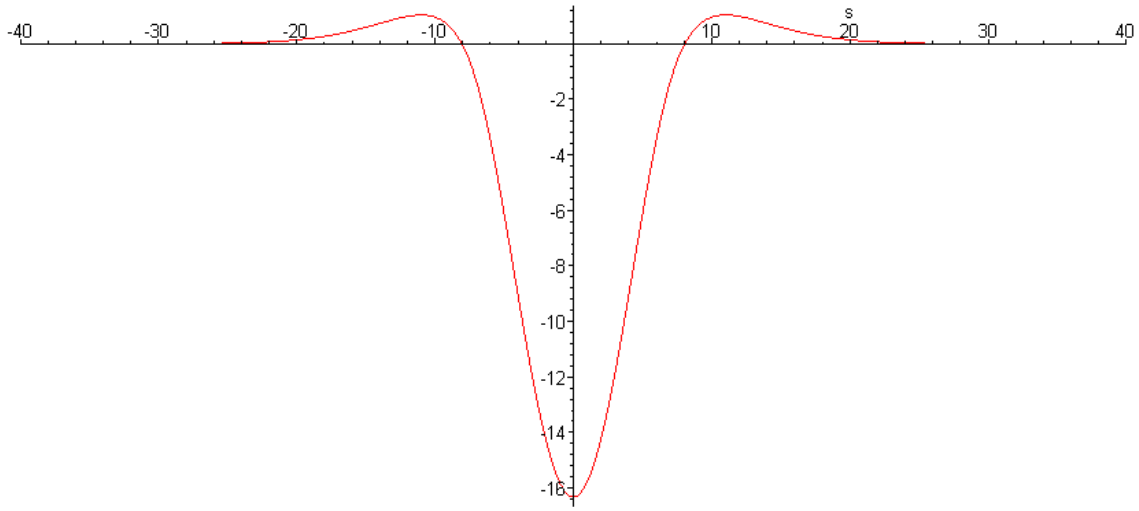

Figure 4.17. $\hat{z}(s) - \hat{y}(s)$ for complex eigenvalue case, $c = .9$, $\gamma = 3.609832084$.

As before, we will also look at the graphs of $\hat{z}(s)$ and $\hat{y}(s)$ separately.

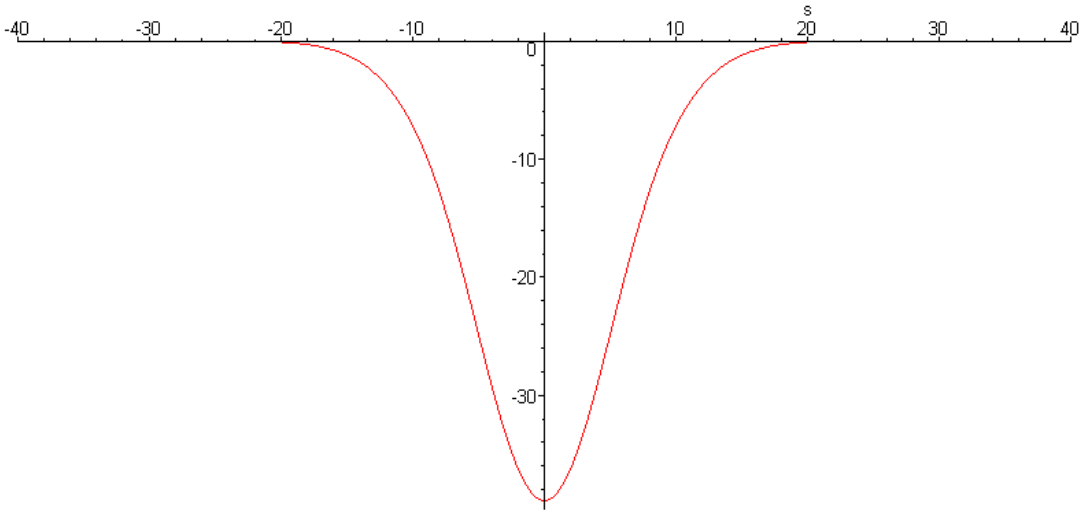

Figure 4.18. $\hat{z}(s)$ for complex eigenvalue case, $c = .9$, $\gamma = 3.609832084$.

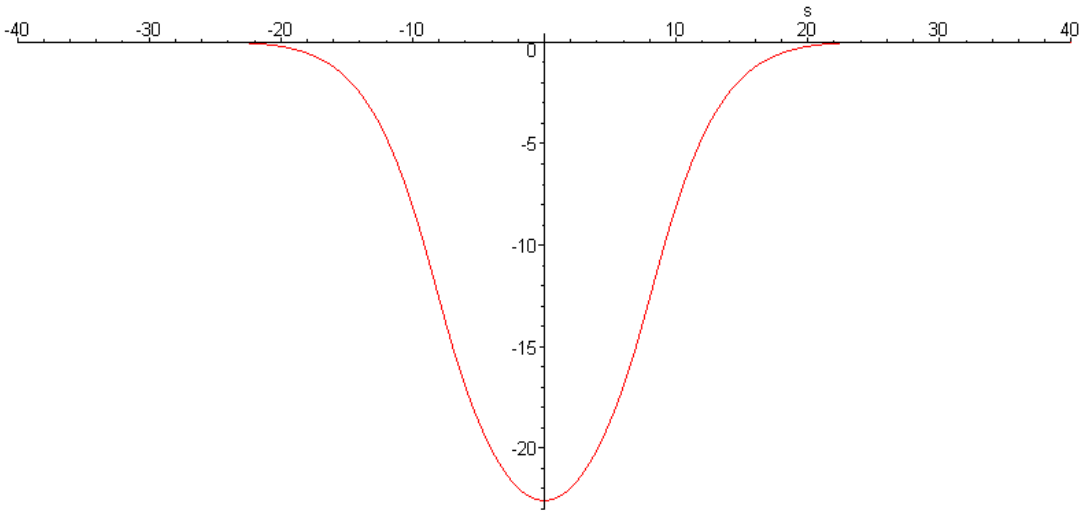

Figure 4.19. $\hat{y}(s)$ for complex eigenvalue case, $c = .9$, $\gamma = 3.609832084$.

We observe that the shape of $\hat{z}(s)$ and $\hat{y}(s)$ are approximately the same as in the real-valued eigenvalue case above. By varying the value of c within this case and computing using the same method as above, we observe the following results.

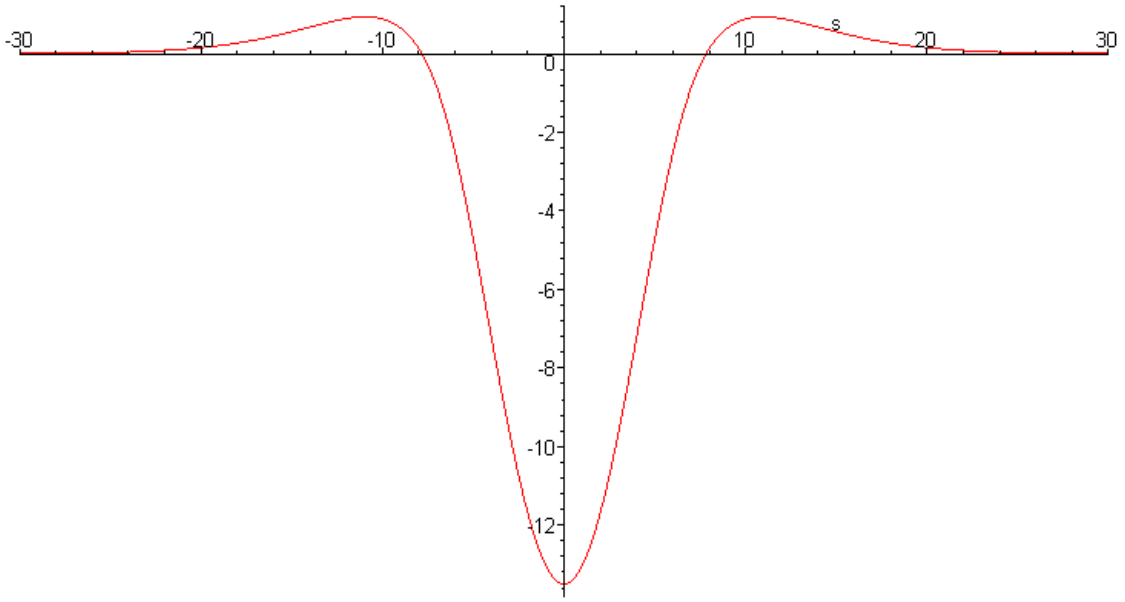

Figure 4.20. $\hat{z}(s) - \hat{y}(s)$ for complex eigenvalue case, $c = .92$, $\gamma = 3.745909006$.

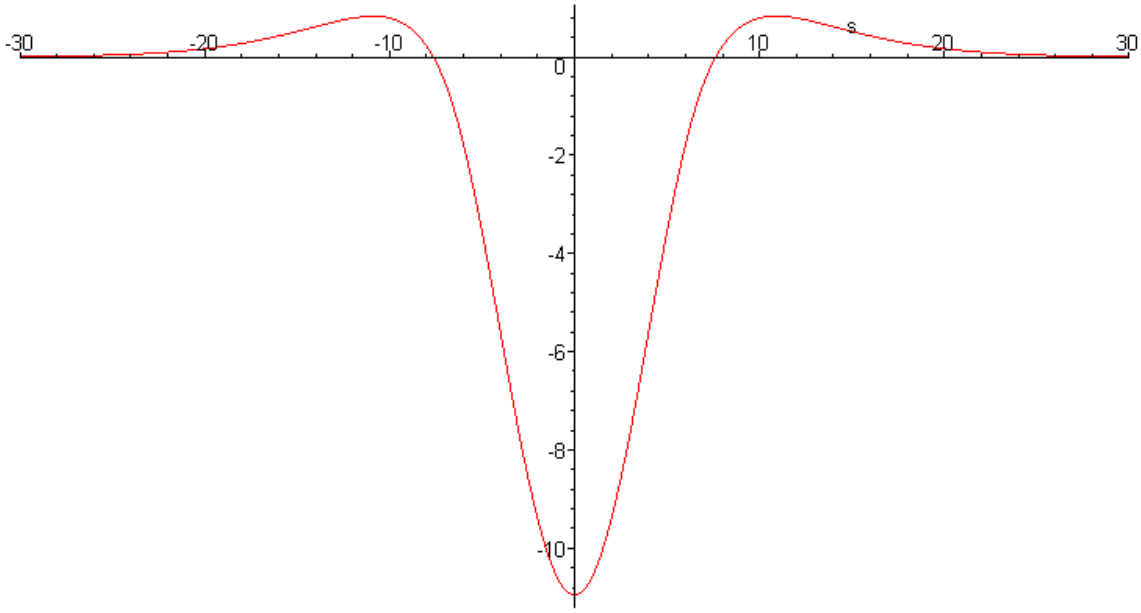

Figure 4.21. $\hat{z}(s) - \hat{y}(s)$ for complex eigenvalue case, $c = .94$, $\gamma = 3.946255431$.

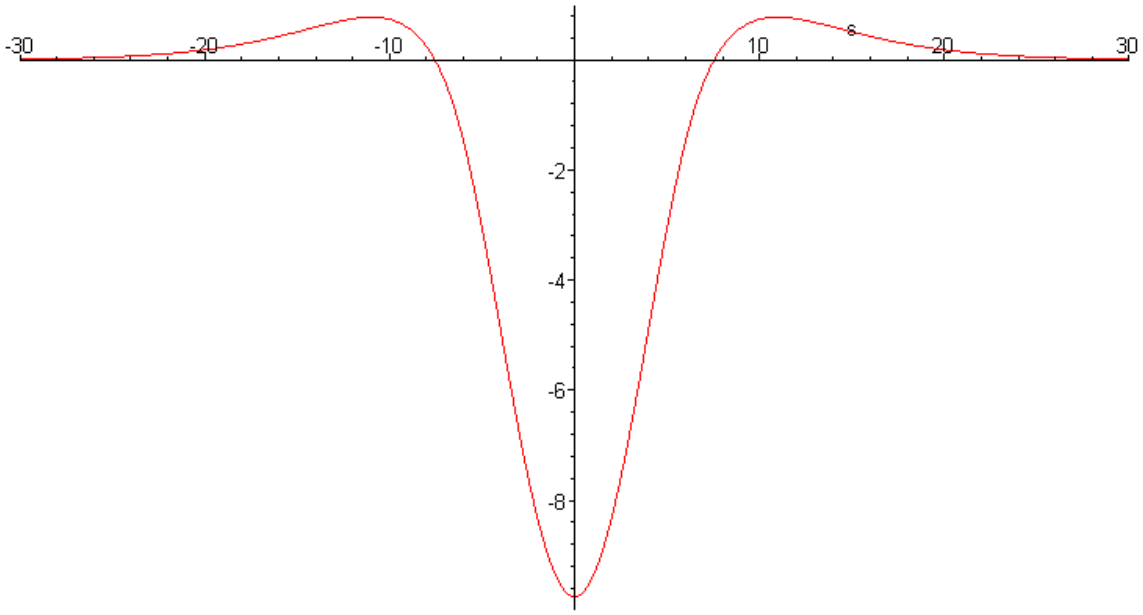

Figure 4.22. $\hat{z}(s) - \hat{y}(s)$ for complex eigenvalue case, $c = .95$, $\gamma = 4.100095431$.

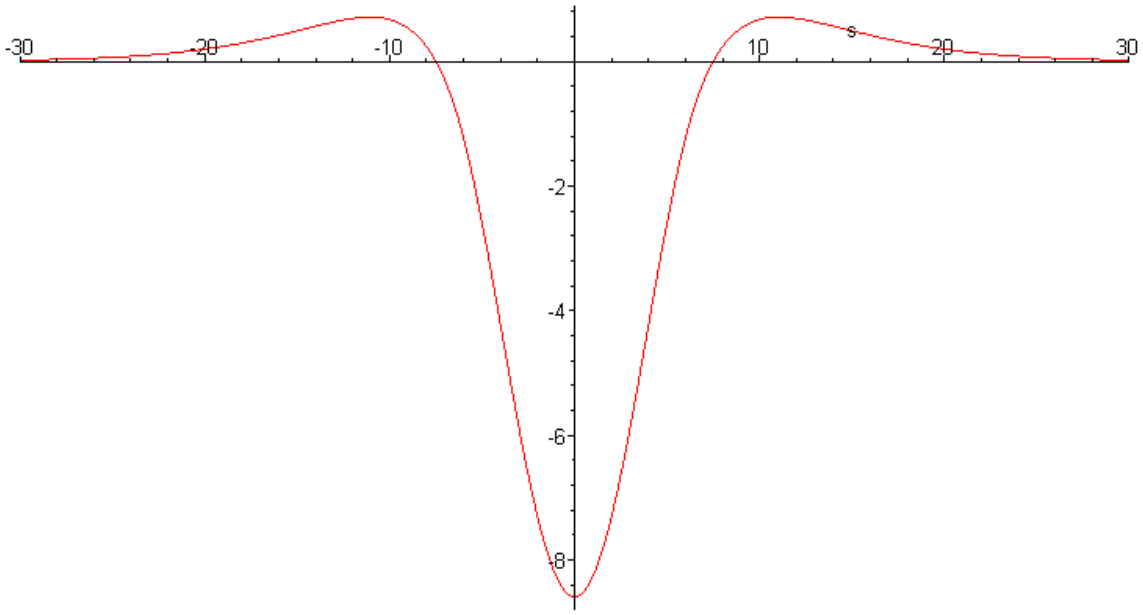

Figure 4.23. $\hat{z}(s) - \hat{y}(s)$ for complex eigenvalue case, $c = .96$, $\gamma = 4.362622238$.

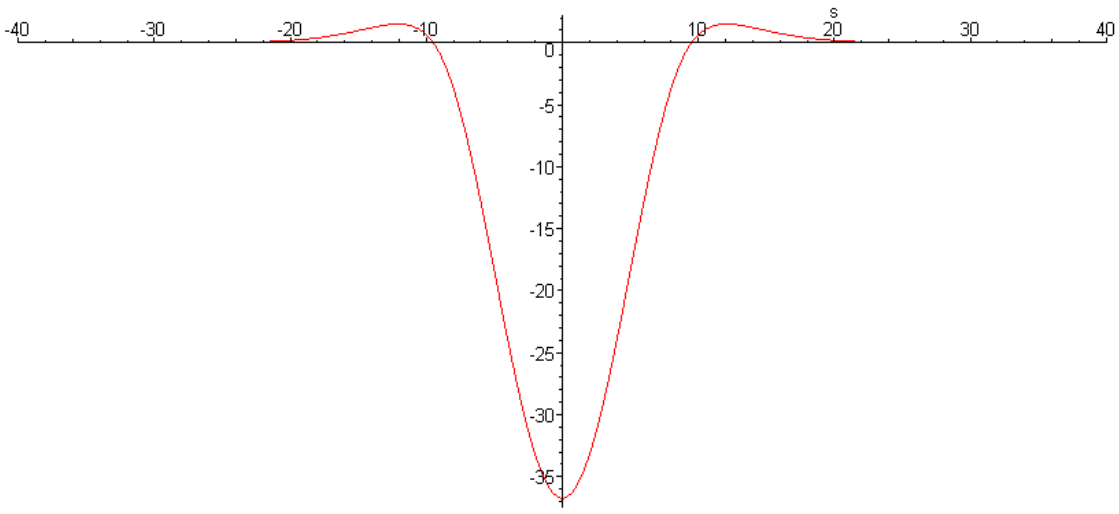

Figure 4.24. $\hat{z}(s) - \hat{y}(s)$ for complex eigenvalue case, $c = .8$, $\gamma = 3.238744281$.

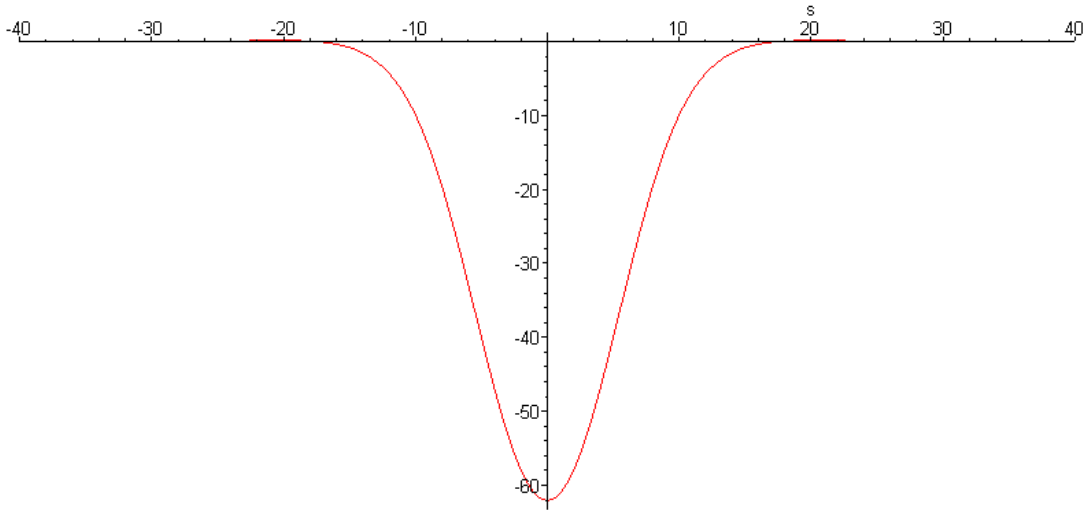

Figure 4.25. $\hat{z}(s)$ for complex eigenvalue case, $c = .8$, $\gamma = 3.238744281$.

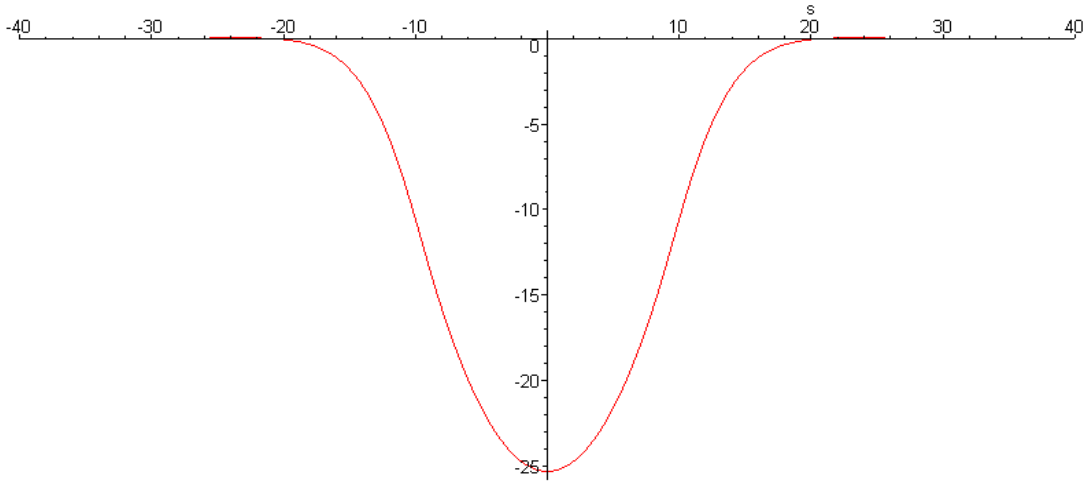

Figure 4.26. $\hat{y}(s)$ for complex eigenvalue case, $c = .8$, $\gamma = 3.238744281$.

Again, we observe that the overall shape of the curves are similar, and that maximum amplitude decreases somewhat as c increases. The last graph represents both the lowest value of c, and the largest amplitude of $\hat{z}(s) - \hat{y}(s)$ observed in either the real- or complex-eigenvalue cases. Further, we note that the values of $\hat{z}(s)$ and $\hat{y}(s)$ are somewhat less than those observed in Figures 4.9 , 4.10, 4.14, and 4.15 above.

As in the real-valued eigenvalue case before, the function that defines our controlling variable has more than one zero. Using methodology similar to what we used in that case, we can check further into this case. For $c = .9$, we look at $f(\gamma)$ on an extended scale.

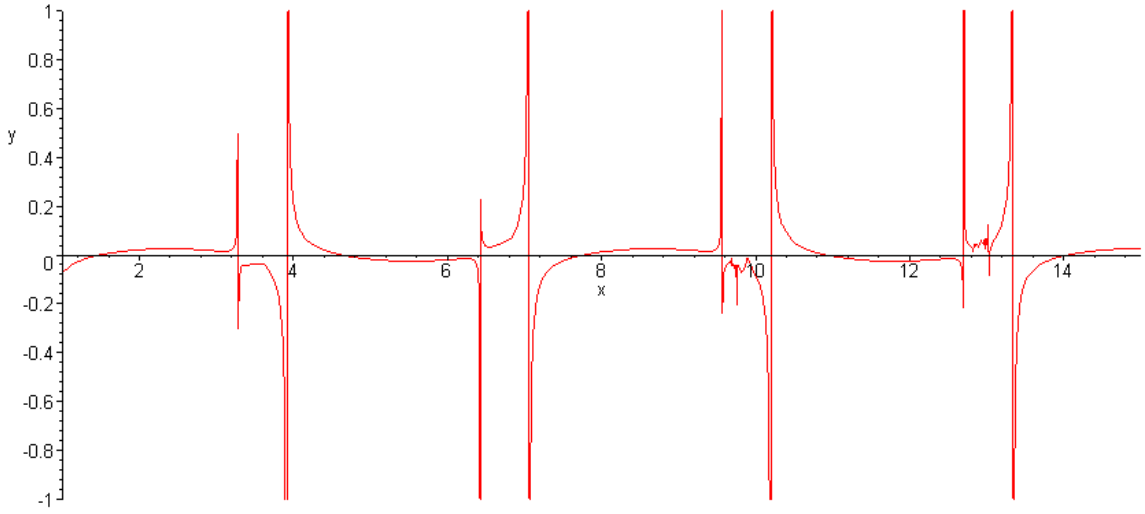

Figure 4.27. $f(\gamma)$ for $c = .9$, extended scale.

We note that the pattern that gave us the zero for our previous solution is between three and four, but that the zero does not appear on this graph, due to the sampling rate of the plot feature in MAPLE. By again changing the scale on the graph, we can focus on parts of the domain that might give additional zeros of the function. Specifically,

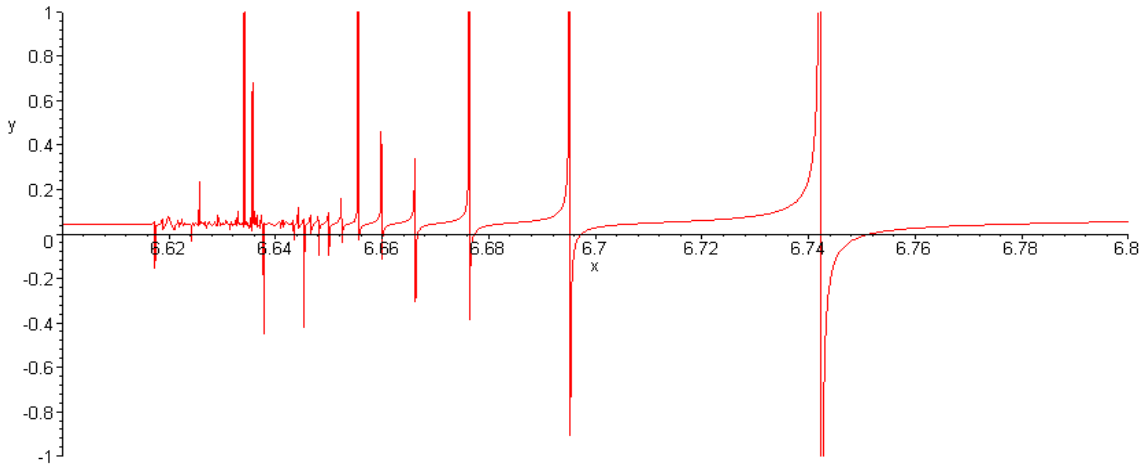

Figure 4.28. $f(\gamma)$ for $c = .9$, restricted scale.

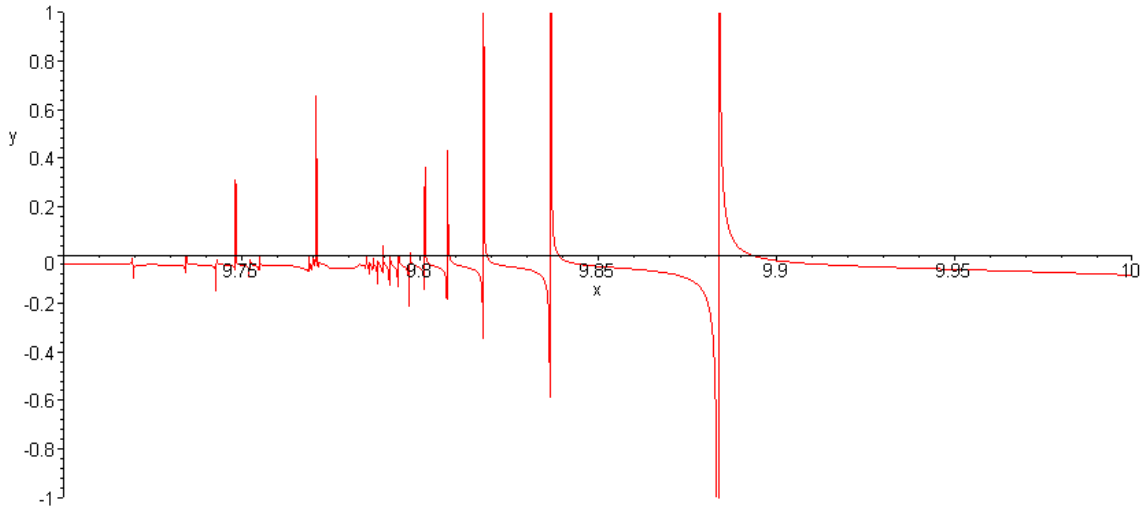

Figure 4.29. $f(\gamma)$ for $c = .9$, restricted scale.

We select the largest zero from each of these graphs, and use MAPLE to get exact values for γ. Our standard methodology gives the following graphs.

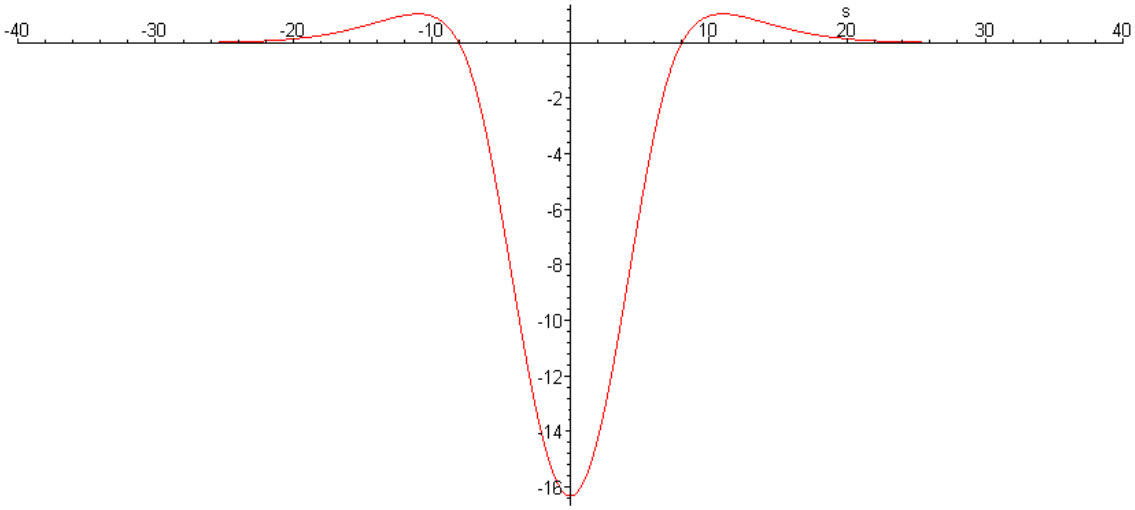

Figure 4.30. $\hat{z}(s) - \hat{y}(s)$ for complex eigenvalue case, $c = .9$, $\gamma = 6.751424738$.

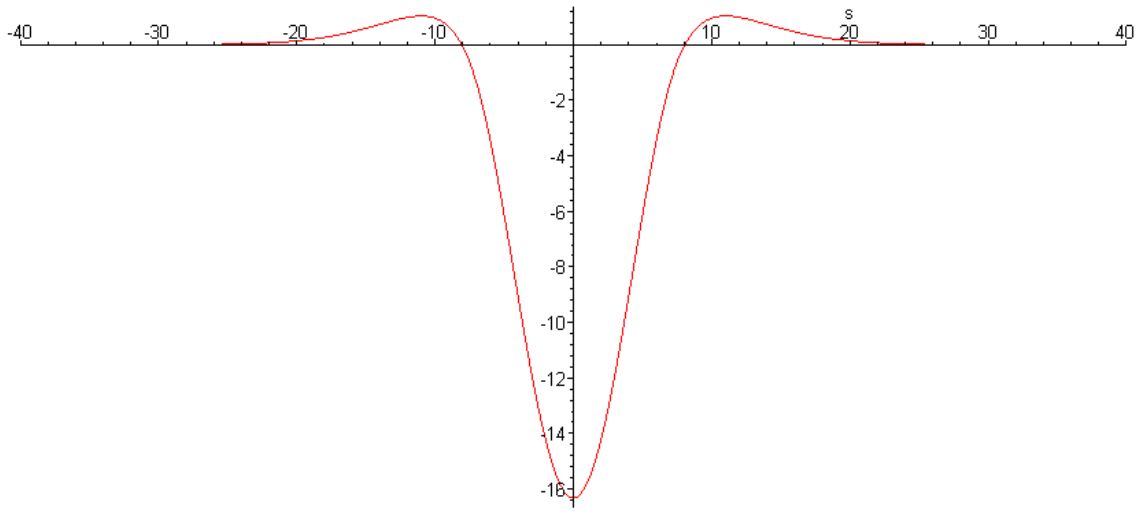

Figure 4.31. $\hat{z}(s) - \hat{y}(s)$ for complex eigenvalue case, $c = .9$, $\gamma = 9.893017391$.

The first observation is that the curves are very similar to the other graphs in this case, as well as almost identical to one another. The second thing is that we might have expected solutions with more oscillatory behavior, as observed in the real eigenvalue case. We continue the investigation by observing two more zeros of $f(\gamma)$ from Figure 4.28 near $\gamma = 6.66$ and $\gamma = 6.65$. By following the established method, we produce the following graphs.

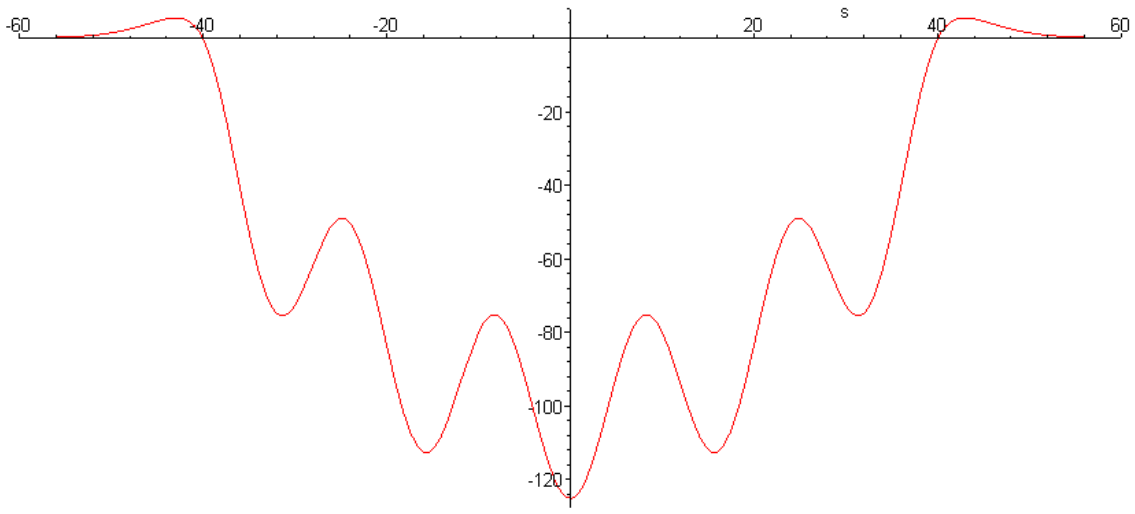

Figure 4.32. $\hat{z}(s) - \hat{y}(s)$ for complex eigenvalue case, $c = .9$, $\gamma = 6.660152836$.

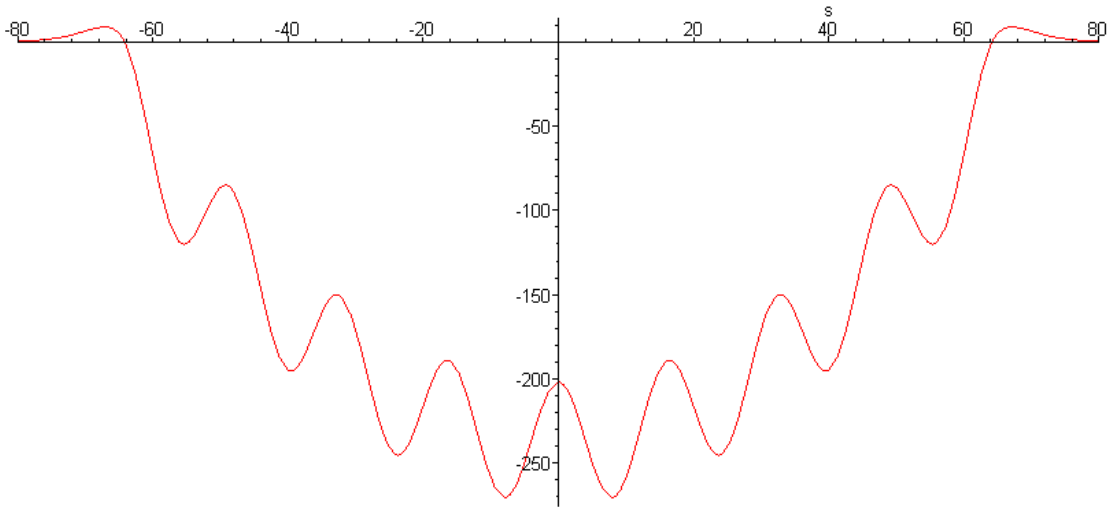

Figure 4.33. $\hat{z}(s) - \hat{y}(s)$ for complex eigenvalue case, $c = .9$, $\gamma = 6.650090665$.

As with other cases, it might be instructive to view $\hat{z}(s)$ and $\hat{y}(s)$ independently. Consider the case shown in Figure 4.33 above.

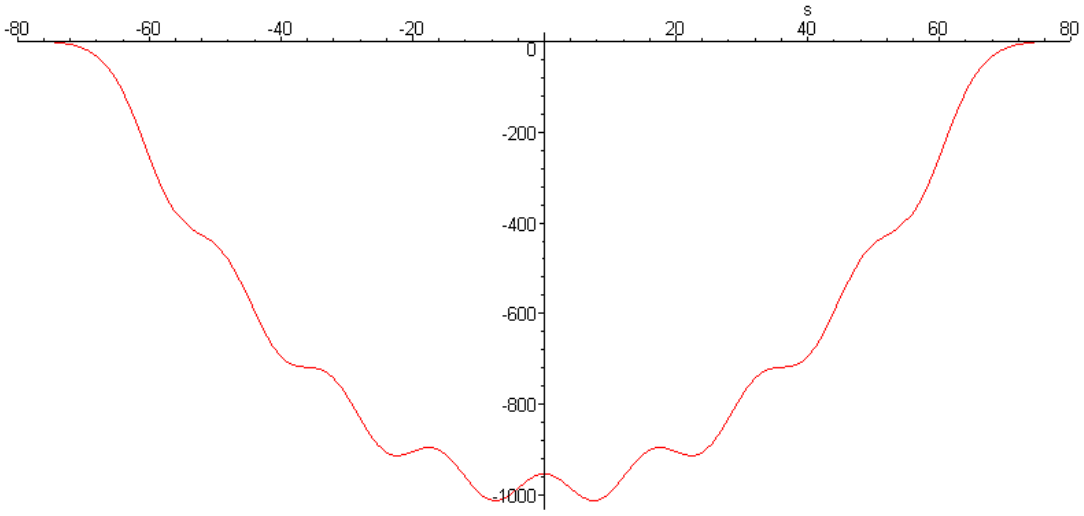

Figure 4.34. $\hat{z}(s)$ for complex eigenvalue case, $c = .9$, $\gamma = 6.650090665$.

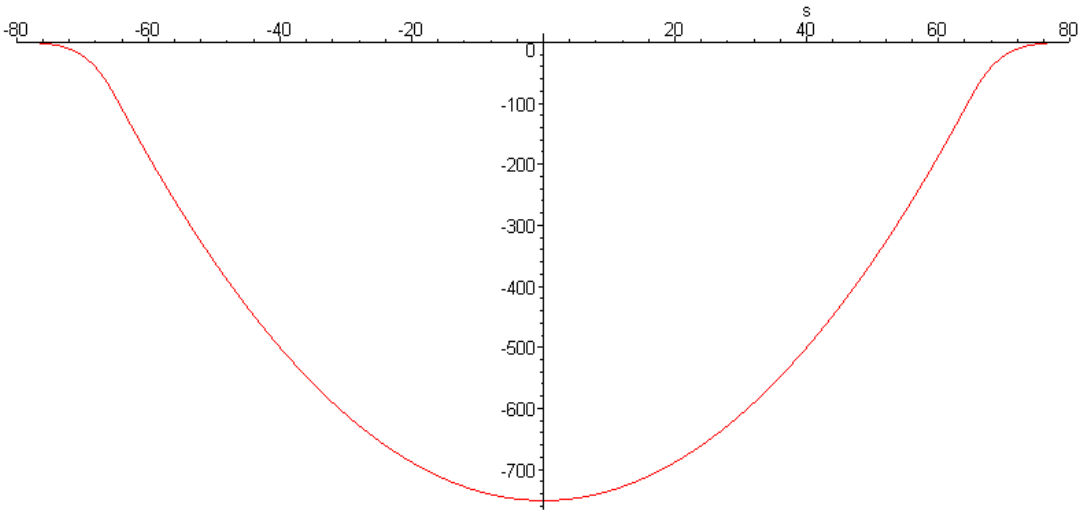

Figure 4.35. $\hat{y}(s)$ for complex eigenvalue case, $c = .9$, $\gamma = 6.650090665$.

These graphs are very interesting, in that they are similar to the graphs from the real eigenvalue case, but are both more variable and of higher amplitude. The additional zeros of the real eigenvalue case generated what appears to be a pattern. The same is true here. The five-peaked graph

corresponds to the fifth zero, counted from the right, in this group. Likewise there is a correspondence between the eight-peaked graph and the eighth zero from the right. This may be a pattern observed in general, or we may have chosen a special case. Also, as noted before, it is possible, probably likely, that at least some of these solutions are of such large amplitude that we would be unable to observe them in an actual suspension bridge.

CHAPTER 5

CONCLUSIONS AND RECOMMENDATIONS

In this thesis, we studied traveling waves in a Lazer-McKenna suspension bridge system. The system is governed by two coupled nonlinear beam and wave equations, and describes the vertical deflections in the roadbed and supporting cable of a suspension bridge. Based on some basic analysis on the system, we are able to compute traveling waves numerically using MAPLE. Multiple large-amplitude traveling waves were obtained, and several graphs of various traveling waves are displayed and discussed in Chapter 4.

Future work on this problem might include investigation of systems with controlling constants from measurements of existing or proposed bridges might be a good place to start. The constants used were not completely arbitrary, but no attempt was made to model a particular bridge system. Such an investigation would no doubt be interesting.

Investigation of various combinations of controlling constants might be a good avenue of inquiry. Such investigation might be done in conjunction with the particular bridge investigation above, or independently. There are a number of constant values that might have a significant effect on the dynamics of the bridge; this investigation would take quite a bit of time and effort. For example, the ratio between the masses of the cable and the roadbed (m_c and m_b) might be a rewarding place to start.

We assumed an undampened system for this thesis. Problems with dampened systems would seem to be an area of interest. The outcome with some degree of dampening might be considerably different. To start, we might consider the effect of a small dampening term on the roadbed, and ignore the dampening on the cable.

APPENDIX I

MAPLE CODE FOR REAL EIGENVALUE CASE

This is the code that produced Figures 4.1-4.4 directly, and Figures 4.5-4.15 with very minor changes.

```
> with(plots);with(linalg); with(DEtools);plotsetup(window); with(student);

> EI:=16;
mb:=3;
mc:=1;
Q:=4;
k0:=Q*Q/EI;
k1:=4*Q*Q/EI;
k:=1;

> c0:=evalf(sqrt(((Q*mb+2.0*sqrt(k*EI)*mc)-
sqrt((Q*mb+2.0*sqrt(k*EI)*mc)*(Q*mb+2.0*sqrt(k*EI)*mc)
+4.0*mb*mc*(k*EI-2.0*Q*sqrt(k*EI))))/(2.0*mb*mc)));

> c1:=sqrt(Q/(mb+mc));
c:=0.9;

> omega:=evalf(c*sqrt(mb/EI));

> F1:=(k*EI-(Q-mc*c*c)*mb*c*c);

> F2:=((Q-mc*c*c)*mb*c*c-k*EI)*((Q-mc*c*c)*mb*c*c-k*EI)-4.0*(Q-
mc*c*c)*k*EI*(Q-(mb+mc)*c*c);

> F3:=evalf(-mb*mc*c*c*c*c+(Q*mb+2.0*sqrt(k*EI)*mc)*c*c+(k*EI-
2.0*Q*sqrt(k*EI)));

> lambda:=sqrt((F1-sqrt(F2))/(2.0*(Q-mc*c*c)*EI));abs(lambda);

> rho:=arctan(Im(lambda)/Re(lambda));

> mu:=x->((Q-mc*c*c)/(((mb+mc)*c*c-
Q)*cos(x)+EI*abs(lambda)*abs(lambda)*cos(x-2*rho)));
```

```
> s0:=x->(-1.*mu(x)*abs(lambda)/k*(mb*c*c*cos(x-
rho)+EI*abs(lambda)*abs(lambda)*cos(x-3.*rho)));

> d1:=x->-1.*k*s0(x)*s0(x)/2./mb/c/c-d3(x)*cos(omega*s0)+mu(x)*cos(x);

> d3:=x->-mu(x)*(abs(lambda))^3*cos(x-3*rho)/omega^3/sin(omega*s0(x));

> f:=x->-
k/mu(x)/mb/c/c+d3(x)*omega^2*cos(omega*s0(x))/mu(x)+abs(lambda)*abs(lamb
da)*cos(x-2*rho);

> plot(f(x),x=1..5,y=-1..1);

> gamma1:=fsolve(f(x)=0,x=3.6..3.8);

> d3:=d3(gamma1);
s0:=s0(gamma1);
mu:=mu(gamma1);
d1:=d1(gamma1);

> z1:=s->exp(s*Re(lambda))*mu*cos(s*Im(lambda)-gamma1);
> y1:=s->-exp(s*Re(lambda))*mu*(mb*c*c*cos(s*Im(lambda)-
gamma1)+EI*abs(lambda)*abs(lambda)*cos(s*Im(lambda)-
gamma1+2*rho))/(mc*c*c-Q);

> z2:=s->d1+k*(s-s0)*(s-s0)/2/mb/c/c+d3*cos(omega*(s-s0));

> y2:=s->(-d1*mb*c*c-(k*(s-s0)*(s-s0))/2-k*EI/mb/c/c)/(mc*c*c-Q);

> D1:=plot((z1(s)-y1(s)),s=-15..0):
> D2:=plot((z2(s)-y2(s)),s=0..2*s0):
> display({D1,D2});

> Z1:=s->exp((s+s0)*Re(lambda))*mu*cos((s+s0)*Im(lambda)-gamma1);
> Y1:=s-> exp((s+s0)*Re(lambda))*mu*(mb*c*c*cos((s+s0)*Im(lambda)-
gamma1)+EI*abs(lambda)*abs(lambda)*cos((s+s0)*Im(lambda)-
gamma1+2*rho))/(mc*c*c-Q);

> Z2:=s->d1+k*s*s/2/mb/c/c+d3*cos(omega*s);

> Y2:=s->(-d1*mb*c*c-(k*s*s)/2-k*EI/mb/c/c)/(mc*c*c-Q);

> D3:=plot((Z1(s)-Y1(s)),s=-40..-s0):
> D4:=plot((Z2(s)-Y2(s)),s=-s0..s0):
> D5:=plot((Z1(-s)-Y1(-s)),s=s0..40):
> display({D3,D4,D5});
```

```
> D6:=plot(Z1(s),s=-40..-s0):
> D7:=plot(Z2(s),s=-s0..s0):
> D8:=plot(Z1(-s),s=s0..40):
> display({D6,D7,D8});

> D9:=plot(Y1(s),s=-40..-s0):
> D10:=plot(Y2(s),s=-s0..s0):
> D11:=plot(Y1(-s),s=s0..40):
> display({D9,D10,D11});
```

APPENDIX II

MAPLE CODE FOR COMPLEX EIGENVALUE CASE

This is the code that produced Figures 4.16-4.19 directly, and Figures 4.20-4.26 with very minor changes.

```
> with(plots);with(linalg); with(DEtools);plotsetup(window); with(student);

> EI:=16;
mb:=3;
mc:=1;
Q:=4;
k0:=Q*Q/EI;
k1:=4*Q*Q/EI;
k:=1;

> c0:=evalf(sqrt(((Q*mb+2.0*sqrt(k*EI)*mc)-
sqrt((Q*mb+2.0*sqrt(k*EI)*mc)*(Q*mb+2.0*sqrt(k*EI)*mc)
+4.0*mb*mc*(k*EI-2.0*Q*sqrt(k*EI))))/(2.0*mb*mc)));

> cmax:=sqrt(Q/(mb+mc));
c:=0.98;

> omega:=evalf(c*sqrt(mb/EI));

> F1:=(k*EI-(Q-mc*c*c)*mb*c*c);

> F2:=((Q-mc*c*c)*mb*c*c-k*EI)*((Q-mc*c*c)*mb*c*c-k*EI)-4.0*(Q-
mc*c*c)*k*EI*(Q-(mb+mc)*c*c);

> F3:=evalf(-mb*mc*c*c*c*c*c+(Q*mb+2.0*sqrt(k*EI)*mc)*c*c+(k*EI-
2.0*Q*sqrt(k*EI)));

> lambda1:=sqrt((F1-sqrt(F2))/(2.0*(Q-mc*c*c)*EI));
lambda2:=sqrt((F1+sqrt(F2))/(2.0*(Q-mc*c*c)*EI));

> d3:=s-
>(k*(lambda1+lambda2*(1+lambda1*s)))/(mb*c*c*omega*((lambda1*lambda2-
omega^2)*sin(omega*s)+omega*(lambda1+lambda2)*cos(omega*s)));
```

```
> c1:=s->1./(lambda2-lambda1)/lambda1^2*(k*lambda2/mb/c^2-
d3(s)*omega^2*(lambda2*cos(omega*s)-omega*sin(omega*s)));
c2:=s->1./(lambda1-lambda2)/lambda2^2*(k*lambda1/mb/c^2-
d3(s)*omega^2*(lambda1*cos(omega*s)-omega*sin(omega*s)));

> d1:=s->c1(s)+c2(s)-k*s^2/2/mb/c^2-d3(s)*cos(omega*s);

> g:=s->((mb+mc)*c*c-Q)/(mc*c*c-Q)*d1(s)+d3(s)*cos(omega*s)+(((mb+mc)*c^2-
Q)*k*s*s+2*k*EI)/2/(mc*c*c-Q)/mb/c/c+1;

> plot(g(s),s=0..10,y=-20..20);

> s0:=fsolve(g(s)=0,s=5..6);

> d3:=d3(s0);
c1:=c1(s0);
c2:=c2(s0);
d1:=d1(s0);

> z1:=s->c1*exp(lambda1*s)+c2*exp(lambda2*s);
> y1:=s->(-mb*c*c*(c1*exp(lambda1*s)+c2*exp(lambda2*s))-
EI*(c1*lambda1*lambda1*exp(lambda1*s)+c2*lambda2*lambda2*exp(lambda2*s
)))/(mc*c*c-Q);

> z2:=s->d1+k*(s-s0)*(s-s0)/2/mb/c/c+d3*cos(omega*(s-s0));

> y2:=s->(-d1*mb*c*c-(k*(s-s0)*(s-s0))/2-k*EI/mb/c/c)/(mc*c*c-Q);

> D1:=plot((z1(s)-y1(s)),s=-15..0):
> D2:=plot((z2(s)-y2(s)),s=0..2*s0):
> display({D1,D2});
> Z1:=s->c1*exp(lambda1*(s+s0))+c2*exp(lambda2*(s+s0));;
> Y1:=s->(-mb*c*c*(c1*exp(lambda1*(s+s0))+c2*exp(lambda2*(s+s0)))-
EI*(c1*lambda1*lambda1*exp(lambda1*(s+s0))+c2*lambda2*lambda2*exp(lamb
da2*(s+s0))))/(mc*c*c-Q);;

> Z2:=s->d1+k*s*s/2/mb/c/c+d3*cos(omega*s);

> Y2:=s->(-d1*mb*c*c-(k*s*s)/2-k*EI/mb/c/c)/(mc*c*c-Q);

> D3:=plot((Z1(s)-Y1(s)),s=-40..-s0):
> D4:=plot((Z2(s)-Y2(s)),s=-s0..s0):
> D5:=plot((Z1(-s)-Y1(-s)),s=s0..40):
> display({D3,D4,D5});
```

```
> D6:=plot(Z1(s),s=-40..-s0):
> D7:=plot(Z2(s),s=-s0..s0):
> D8:=plot(Z1(-s),s=s0..40):
> display({D6,D7,D8});

> D9:=plot(Y1(s),s=-40..-s0):
> D10:=plot(Y2(s),s=-s0..s0):
> D11:=plot(Y1(-s),s=s0..40):
> display({D9,D10,D11});
>
```

REFERENCES

[1] A. M. Abdel-Ghaffer, *Suspension bridge vibration: continuation formulation*, J. Engrg. Mech., 108(1982), pp. 1215-1232

[2] N. U. Ahmed and H. Harbi, *Mathematical analysis of dynamic models of suspension bridges*, SIAM J. Appl. Math., 58(1998), pp. 853-874

[3] O. H. Amann, T von Karman, and G. B. Woodruff, *The Failure of the Tacoma Narrows Bridge*, Federal Works Agency, Washington, D.C., 1941

[4] J. Berkovits, P. Drabek, H. Leinfelder, V. Mustonen, and G. Tajcova, *Time periodic oscillations in suspension bridges: existence of unique solutions*, Nonlinear Anal. Real World Appl., 1(2000), pp. 345-362

[5] F. Bleich, C. B. McCollough, R. Rosencrans, and G. S. Vincent, *The Mathematical Theory of Suspension Bridges*, Bureau of Public Roads, U. S. Dept. of Commerce, Washington, D.C., 1950

[6] Y. Chen and P. J. McKenna, *Traveling waves in a nonlinearly suspended beam: Theoretical results and numerical observations*, J. Differential Equations, 136 (1997), pp. 325-355

[7] Q. H. Choi, T. Jung, and P. J. McKenna,*The study of a nonlinear suspension bridge equation by a variational reduction method*, Appl. Anal., 50(1993), pp. 73-92

[8] Z. Ding, *Nonlinear periodic oscillations in suspension bridges*, in Control of Nonlinear Distriduted Systems, Lecture Notes in Pure and Appl. Math. 218, Marcel Dekker, NY, 2000, pp. 69-84

[9] Z. Ding, *Nonlinear periodic oscillations in a suspension bridge system under periodic external aerodynamic forces*, Nonlinear Anal., 49(2002), pp. 1079-1097

[10] Z. Ding*, On nonlinear oscillations in a suspension bridge system*, Trans. Amer. Math. Soc., 354(2002), pp. 265-274

[11] Z. Ding, *Multiple periodic oscillations in a nonlinear suspension bridge system*, J. Math. Anal. Appl., 269(2002), pp 726-746

[12] Z. Ding, *Traveling Waves in a Suspension Bridge System*, SIAM J. Math. Anal., 35 (2003), pp. 160-171

[13] P. Drabek and H. Leinfelder, *Coupled string-beam equations as a model of suspension bridges*, Appl. Math. 44(1999), pp. 97-142

[14] J. Glover, A. C. Lazer, and P. J. McKenna, *Existence and stability of large scale nonlinear oscillations in suspension bridges*, Z. Agnew. Math. Phys., 40(1989), pp. 172-200

[15] J. Horak and P. J. McKenna, *Traveling Waves in Nonlinearly Supported Beams and Plates*, Prog. Nonlinear Diff. Equations, 54(2003), pp. 197-215

[16] L. D. Humphreys, *Numerical mountain pass solutions of a suspension bridge equation*, Nonlinear Anal., 28(1997), pp. 1811-1826

[17] L. D. Humphreys and P. J. McKenna, *Multiple periodic solutions for a nonlinear suspension brige equation*, IMA J. Appl. Math., 63(1999), pp 37-49

[18] L. D. Humphreys and P. J. McKenna, *When a Mechanical Model Goes Nonlinear: Unexpected Responses to Low-Periodic Shaking*, Amer. Math. Monthly, 112(2005), pp. 861-875

[19] S. Johnson and R. T. Leon, *Encyclopedia of Bridges and Tunnels*, Facts on File, NY, 2002

[20] A. C. Lazer and P. J. McKenna, *Large scale oscillation behavior in loaded asymmetric systems*, Ann. Inst. H. Poincare Anal. Non Lineare, 4(1987), pp. 243-274

[21] A. C. Lazer and P. J. McKenna, *Large Amplitude Periodic Oscillations in Suspension Bridges: Some New Connections with Nonlinear Analysis*, SIAM Rev. 32 (1990), pp. 537-578

[22] P. J. McKenna and W. Walter, *Nonlinear oscillations in a suspension bridge* , Arch. Ration. Mech. Anal., 98(1987), pp. 167-177

[23] P. J. McKenna and W. Walter, *Travelling Waves in a Suspension Bridge*, SIAM J. Appl. Math. 50 (1990), pp. 703-715

[24] B. Pittel and V. Jakubivic, *A mathematical analysis of the stability of suspensions bridges based on the example of the Tacoma bridge*, Vsetnik Liningrad. Univ., 24(1969), pp. 81-90

[25] R. H. Scanlan, *The action of flexible bridges under wind. Part I: Flutter theory*, J. Sound Vibration, 60(1978), pp.187-199

[26] R. H. Scanlan, *The actions of flexible bridges under wind, Part II: Buffeting theory*, J. Sound Vibration, 60(1978), pp. 201-211

[27] A. Selberg, *Oscillation and aerodynamic stability of suspension bridges*, Acta Polytech. Scand., 13(1961), pp. 308-377

[28] E. G. Wiles, *Report of aerodynamic studies on proposed San Pedro-Terminal Island suspension bridge, California*, Research, Bureau of Public Roads, U. S. Dept. of Commerce, Washington, D. C., 1960

VITA

Graduate College
University of Nevada, Las Vegas

Robert A. Ain, Jr.

Degree:

Bachelor of Science, Basic Sciences, 1974
United States Air Force Academy

Thesis Title: Traveling Waves in a Suspension Bridge System

Thesis Committee:

Chairman, Dr. Zhonghai Ding, PhD.
Committee Member, Dr. David Costa, PhD.
Committee Member, Dr. George Miel, PhD.
Graduate Faculty Representative, Dr. Yitung Chen, PhD.